PHYSICAL REVIEW D **96,** 074011 (2017)

Bose-Einstein correlations in perturbative QCD: v_n dependence on multiplicity

E. Gotsman[1,*] and E. Levin[1,2,†]

[1]*Department of Particle Physics, School of Physics and Astronomy, Raymond and Beverly Sackler Faculty of Exact Science, Tel Aviv University, Tel Aviv 69978, Israel*
[2]*Departemento de Física, Universidad Técnica Federico Santa María, and Centro Científico- Tecnológico de Valparaíso, Avda. Espana 1680, Casilla 110-V, Valparaíso, Chile*

(Received 7 June 2017; published 13 October 2017)

In this paper we study the dependence of Bose-Einstein correlations on the multiplicity of an event. We find that events with large multiplicity stem from the production of several-parton showers, while the additional production of small multiplicity in the central rapidity region (central diffraction) gives a negligible contribution due to emission of soft gluons, which leads to the Sudakov suppression of the exclusive production of two-gluon jets. Hence, the Bose-Einstein correlation is the main source of the azimuthal angle correlations which generate v_n with odd and even n. We find that without this suppression, the measurement of an event with given multiplicity yields $v_{n,n} < 0$ for odd n. It appears that in hadron-nucleus and nucleus-nucleus collisions, the Bose-Einstein correlations do not depend on multiplicity, while for hadron-hadron scattering such dependence can be considerable. We propose a simple Kharzeev-Levin-Nardi type model to describe the dependence of azimuthal angle correlations on the centrality of the event in ion-ion collisions.

DOI: 10.1103/PhysRevD.96.074011

I. INTRODUCTION

In this paper we continue to discuss the Bose-Einstein correlations of gluons as being the main source of the strong azimuthal angle (φ) correlations that have been observed experimentally in nucleus-nucleus, hadron-nucleus, and hadron-hadron collisions [1–11]. It has been known for some time in the framework of Gribov-Pomeron calculus that the Bose-Einstein correlations which stem from the exchange of two Pomerons lead to azimuthal angle correlations [12] (see also Ref. [13]), which do not depend on the rapidity difference between measured hadrons [large range rapidity (LRR) correlations]. In the framework of QCD, these azimuthal correlations originate from the production of two-parton showers, and have been rediscovered in Refs. [14–18] (see also Refs. [19,20]). In Ref. [21] it was demonstrated that Bose-Einstein correlations generate v_n with even and odd n, with values which are close to the experimentally observed ones.

The goal of this paper is to answer three questions: (i) Is the symmetry $\varphi \to \pi - \varphi$ an inherent property of QCD, or of the color glass condensate (CGC) approach, which is the effective theory of QCD at high energies, or it is based on the model assumptions? (ii) What is the multiplicity dependence of the azimuthal angle correlations which stem from the Bose-Einstein ones? (iii) Is it possible to build a simple Kharzeev-Levin-Nardi (KLN)-type [22–28] approach to describe azimuthal correlations in nucleus-nucleus collisions?

The following are our answers to these questions: The symmetry $\varphi \to \pi - \varphi$ is not a general feature of the QCD (or CGC) approach. It does not stem from the Bose-Einstein correlations of identical gluons, and can only appear in measurements that mix events with different multiplicities. In the case of hadron-hadron collisions, for example, such symmetry exists in the Born approximation of perturbative QCD, and could only be measured, if experimentally the central diffraction production and the event with double multiplicity ($n = 2\bar{n}$, where $\bar{n}$ is the average multiplicity in inclusive production) are measured and summed. However, the emission of soft gluons for the central exclusive production in the double log approximation of perturbative QCD leads to a Sudakov form factor which suppress this contribution. Therefore, the Bose-Einstein correlations prevail, leading to $v_n \neq 0$ for odd n, even in totally inclusive measurements, without selection of an event with given multiplicities.

We expect a very mild dependence of v_n on the multiplicity of the observed events. We suggest a model for the Bose-Einstein correlations in heavy ion collisions in the spirit of the KLN approach, which is based on the concept of constructing the simplest model that takes into account the discussed phenomena: in our case, the saturation of the gluon density and the Bose-Einstein correlations.

The double inclusive cross section of two identical gluons has the following general form:

*gotsman@post.tau.ac.il
†leving@post.tau.ac.il, eugeny.levin@usm.cl

$$\frac{d^2\sigma}{dy_1 dy_2 d^2p_{T1} d^2p_{T2}}(\text{identical gluons}) = \frac{d^2\sigma}{dy_1 dy_2 d^2p_{T1} d^2p_{T2}}(\text{different gluons}) \times (1 + C(L_c|\boldsymbol{p}_{T2} - \boldsymbol{p}_{T1}|)) \quad (1)$$

where $C(L_c|\boldsymbol{p}_{T2} - \boldsymbol{p}_{T1}|)$ denotes the correlation function and L_c the correlation length.

In Eq. (1) we denote as identical gluons, two gluons with momenta $\boldsymbol{p}_{T1}$ and $\boldsymbol{p}_{T2}$ that have the same color and the same helicity. The two gluons with the same momenta, but for which we do not impose any restrictions on their colors and helicities, we call "different" gluons. Equation (1) is in accord with the Hanbury Brown and Twiss formula (see Refs. [29,30])

$$\frac{d^2\sigma}{dy_1 dy_2 d^2p_{T1} d^2p_{T2}}(\text{identical gluons}) \propto \langle 1 + e^{ir_\mu Q_\mu}\rangle \quad (2)$$

where averaging $\langle \ldots \rangle$ includes the integration over $r_\mu = r_{1,\mu} - r_{2,\mu}$. There is only one difference: $Q_\mu = p_{1,\mu} - p_{2,\mu}$ degenerates to $\boldsymbol{Q} \equiv \boldsymbol{p}_{T,12} = \boldsymbol{p}_{T2} - \boldsymbol{p}_{T1}$, as the production of two gluons from the two-parton showers does not depend on rapidities.

Equation (2) allows us to measure the typical r_μ of the interaction, or in other words, L_c in Eq. (1) is determined by the typical volume of the interaction. Therefore, we expect several typical L_c: the size of the nucleus R_A; the nucleon size R_N; and the typical size, related to the saturation scale ($r_{\rm sat} = 1/Q_s$, where Q_s denotes the saturation scale [31]). Indications of all these sizes have been seen in Bose-Einstein correlations (see Refs. [17,21]). Using Eq. (1), we can find v_n, since

$$\frac{d^2\sigma}{dy_1 dy_2 d^2p_{T1} d^2p_{T2}} \propto 1 + 2\sum_n v_{n,n}(p_{T1}, p_{T2}) \cos(n\varphi), \quad (3)$$

where φ is the angle between $\boldsymbol{p}_{T1}$ and $\boldsymbol{p}_{T2}$. v_n is determined from $v_{n,n}(p_{T1}, p_{T2})$

$$\text{(a)}\ v_n(p_T) = \sqrt{v_{n,n}(p_T, p_T)};$$
$$\text{(b)}\ v_n(p_T) = \frac{v_{n,n}(p_T, p_T^{\rm Ref})}{\sqrt{v_{n,n}(p_T^{\rm Ref}, p_T^{\rm Ref})}}; \quad (4)$$

Equations (4a) and (4b) depict two methods of how the values of v_n have been extracted from the experimentally measured $v_{n,n}(p_{T1}, p_{T2})$. $p_T^{\rm Ref}$ denotes the momentum of the reference trigger. These two definitions are equivalent if $v_{n,n}(p_{T1}, p_{T2})$ can be factorized as $v_{n,n}(p_{T1}, p_{T2}) = v_n(p_{T1})v_n(p_{T2})$.

II. SYMMETRY $\varphi \to \pi - \varphi$ ($v_n = 0$ FOR ODD n) FOR DIFFERENT MULTIPLICITIES OF PRODUCED HADRONS

A. The Bose-Einstein correlation function for deuteron-deuteron scattering with the correlation length $L_c \propto R_D$

First, we consider the simplest diagram in the Born approximation of perturbative QCD, which we have discussed in Ref. [17] [see Fig. 1(a)]. This diagram describes the interference between two identical gluons in the process of multiparticle production, or in other words, in the processes of the production of two-parton showers. In this diagram $Q_T \propto 1/R_D$ and $|\boldsymbol{Q}_T - \boldsymbol{p}_{12,T}| \propto 1/R_D$, where R_D denotes the deuteron radius, which is much larger than the size of the proton, R_N. Momenta k_T, l_T, $p_{1,T}$, and $p_{2,T}$ in this diagram are of the order of $1/R_N \gg 1/R_D$, and therefore we can neglect Q_T as well as $p_{12,T}$ in the diagram. Bearing this in mind, we see that the correlation function $C(L_c|\boldsymbol{p}_{12,T}|)$ is equal to

$$C(L_c|\boldsymbol{p}_{12,T}|) = \frac{1}{N_c^2 - 1}\frac{\int d^2Q_T G_D(Q_T) G_D(\boldsymbol{Q}_T - \boldsymbol{p}_{12,T})}{\int d^2Q_T G_D(Q_T) G_D(Q_T)}$$
$$\text{with}\quad G_D(Q_T) = \int d^2r e^{i\boldsymbol{r}\cdot\boldsymbol{Q}_T}|\Psi_D(r)|^2, \quad (5)$$

where r denotes the distance between the proton and the neutron in the deuteron.

Equation (5) displays no symmetry with respect to $\varphi \to \pi - \varphi$. However, we can add a different diagram of Fig. 1(b), which describes the central diffraction production of two different gluons in a colorless state.[1] This diagram depends on $\boldsymbol{p}_{1,T} + \boldsymbol{p}_{2,T}$ and generates the correlation function

$$\tilde{C}(L_c|\boldsymbol{p}_{1,T} + \boldsymbol{p}_{2,T}|) \propto \frac{1}{N_c^2 - 1}\frac{\int d^2Q_T G_D(Q_T) G_D(\boldsymbol{Q}_T - \boldsymbol{p}_{1,T} - \boldsymbol{p}_{2,T})}{\int d^2Q_T G_D(Q_T) G_D(Q_T)} \quad (6)$$

since in this diagram Q_T and $\boldsymbol{Q}_T - \boldsymbol{p}_{1,T} - \boldsymbol{p}_{2,T}$ are of the order of $1/R_D$, while k_T, l_T, $p_{1,T}$ and $p_{2,T}$ in this diagram are of the order of $1/R_N \gg 1/R_D$, therefore, we can neglect Q_T as well as $\boldsymbol{p}_{1,T} + \boldsymbol{p}_{2,T}$ in the diagram or, in other words, we can put $\boldsymbol{p}_{1,T} = -\boldsymbol{p}_{2,T}$. After this substitution, both diagrams have the same expressions.

Therefore, if diagrams of Figs. 1(a) and 1(b) have the same weight, the sum will have the symmetry with respect to $\boldsymbol{p}_{2,T} \to -\boldsymbol{p}_{2,T}$, restoring the symmetry with respect to $\varphi \to \pi - \varphi$. At first sight, this is the case since all integrations over k_T and l_T look the same. However, in these two diagrams this is certainly not the case due to different integration with respect to k_- and l_- (or k^+ and l^+).

[1] In the approach seen in Ref. [16] this diagram restores the symmetry $\phi \to \pi - \phi$.

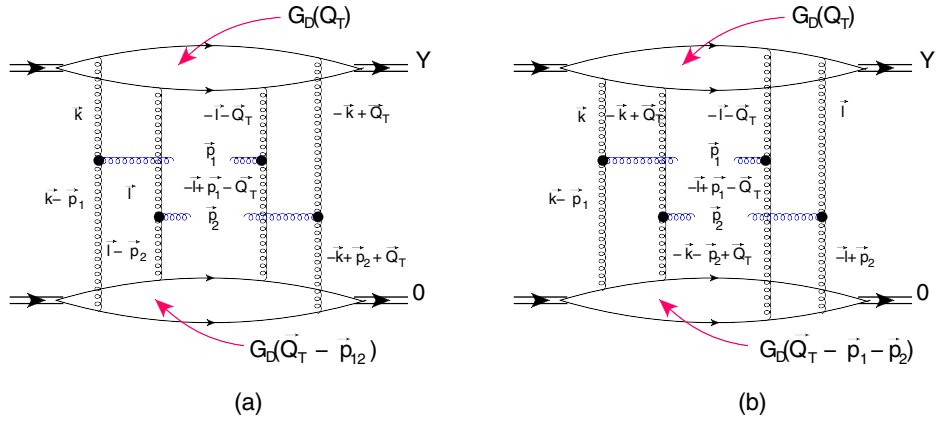

FIG. 1. Deuteron-deuteron scattering in the Born approximation of perturbative QCD: Fig. 1(a) describes the interference diagrams in the production of two identical gluons in the process of multiparticle generation that gives rise to the correlation function $C(L_c|\boldsymbol{p}_{12,T}=\boldsymbol{p}_{1,T}-\boldsymbol{p}_{2,T}|)$; Fig. 1(b) corresponds to the central diffraction of two gluons with different color charges in the colorless state.

This integration generates $1/4$ suppression of the diagram of Fig. 1(b) with respect to the diagram of Fig. 1(a). It is a well-known fact first discussed in the Abramovsky-Gribov-Kancheli (AGK) paper of Ref. [32], as well as in most reviews and books that are devoted to high energy scattering (in particular, those where one of us is an author [31,33,34]). For completeness we discuss this integration in Appendix A.

However, we found it instructive to discuss the contribution of these two diagrams in the framework of the AGK cutting rules, which is the technique that we will use in considering the dependence of the correlation function on multiplicity of produced particles. First, accounting for emission of the gluons with rapidities larger than y_1 and smaller than y_2, and considering $\bar{\alpha}_S|y_1-y_2|\ll 1$, we can describe the two-partonic shower contribution in deuteron-deuteron scattering by the diagrams of Figs. 2(a) and 2(b).

The AGK cutting rules describe the relative contributions of different processes that stem from two–BFKL Pomeron [36,37] exchange. Figure 3(a) describes the elastic scattering, Fig. 3(b) the one-parton shower production, which is screened by the BFKL Pomeron exchange. Figure 3(c) is the production of two-parton showers. The AGK cutting rules state that the cross sections of these three processes are related as $1:-4:2$. The sum of these processes is equal to -1, leading to the negative contribution to the total cross section of two-Pomeron exchange. These rules have a rather general origin based on the unitarity constraints and physical properties of the Pomerons. Indeed, the unitarity constraint has the following form:

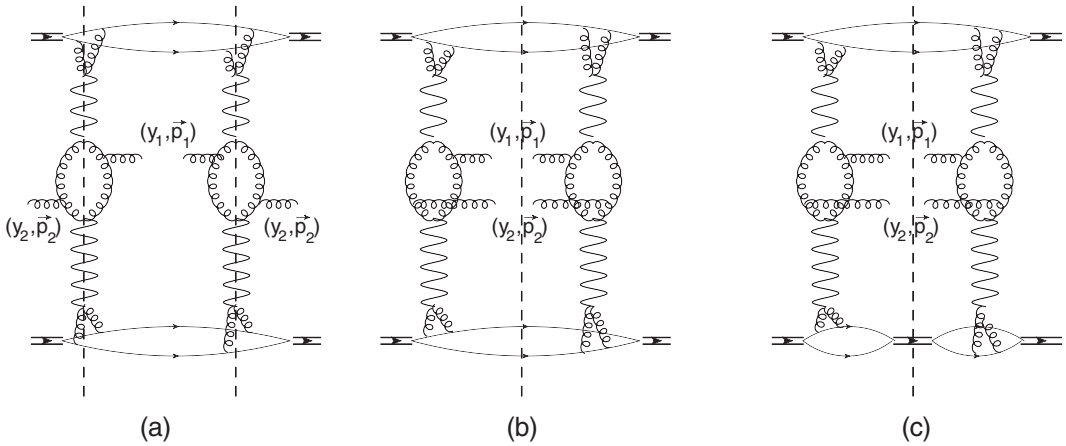

FIG. 2. Mueller diagrams [35] for two-parton shower production of gluons: Fig. 2(a) describes the interference diagrams in the production of two identical gluons in the process of multiparticle production that generates the correlation function $C(L_c|\boldsymbol{p}_{12,T})$; Fig. 2(b) corresponds to central diffraction of two gluons with different color charges in the colorless state; Fig. 2(c) describes the central diffractive production with a different final state, where one deuteron remains intact. The wavy line stands for the BFKL Pomeron [36]. Helical lines correspond to gluons. The vertical dashed lines show the cuts.

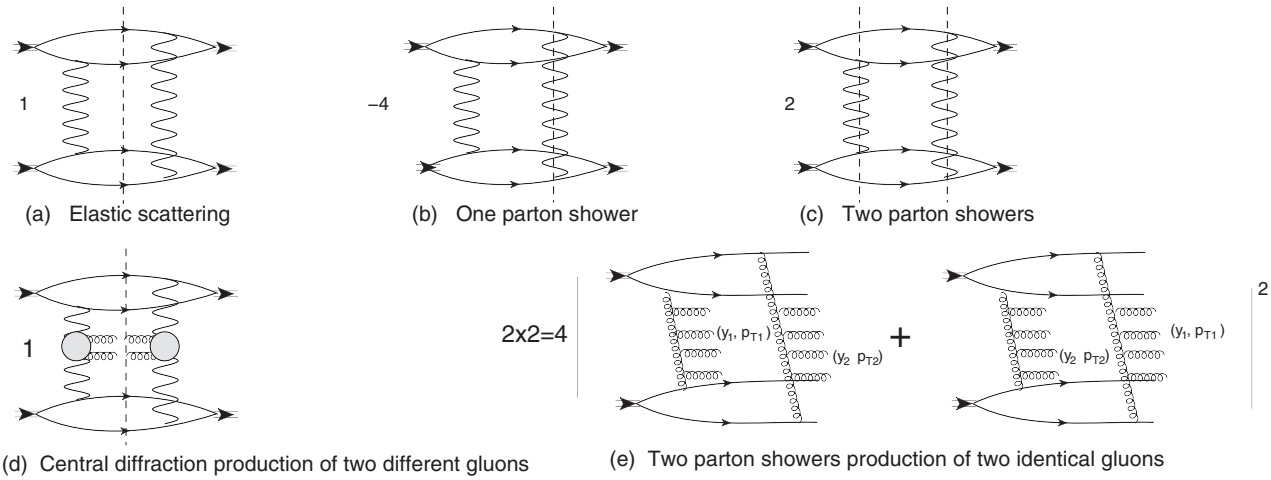

FIG. 3. AGK cutting rules for the exchange of two BFKL Pomerons [Figs. 3(a)–(c)] and the contributions of the central [Fig. 3(d)] and two-parton shower production [Fig. 3(e)] of two gluons.

$$2\mathrm{Im}A_{el}(s,b;i) = \underbrace{|A_{el}(s,b;i)|^2}_{\text{elastic cross section}} + \underbrace{G(s,b,i)}_{\text{contribution of inelastic processes}} \tag{7}$$

where $W=\sqrt{s}$ denotes the energy of the collision, b is impact parameter, and i the set of other quantum numbers that diagonalize the interaction matrix.

For the BFKL Pomeron, the elastic cross section is much smaller than the exchange of a single Pomeron, and Eq. (7) takes the form

$$2\mathrm{Im}P^{\mathrm{BFKL}}(s,b,i) = \underbrace{G^{\mathrm{BFKL}}(s,b,i)}_{\text{cut Pomeron}} \tag{8}$$

Using Eq. (8), one can see that

$$\begin{aligned}
&\sigma_{el} \propto |P^{\mathrm{BFKL}}(s,b,i)|^2;\\
&\sigma_{\text{one parton shower}} \propto -2P^{\mathrm{BFKL}}G^{\mathrm{BFKL}}(s,b,i);\\
&\sigma_{\text{two parton showers}} \propto -\frac{1}{2}G^{\mathrm{BFKL}}(s,b,i)G^{\mathrm{BFKL}}(s,b,i);
\end{aligned} \tag{9}$$

where $\frac{1}{2}$ in the last term stems from the fact that the two cut Pomerons are identical. Using Eq. (8), one reproduces the AGK cutting rules of Figs. 3(a)–3(c).

The central diffraction production of two gluons is shown in the diagram of Fig. 3(a) (elastic scattering), while the interference diagram, which generates the Bose-Einstein correlations, originates from Fig. 3(c) with the extra factor 2, which reflects the fact that the gluon with rapidity—say, y_1—can be produced from two different parton cascades [see Fig. 3(e)]. The processes of central diffractive production are suppressed by a factor of 4 compared to the Bose-Einstein correlations.

To complete the discussion of the possible restoration of $\varphi \to \pi - \varphi$ symmetry due the processes of the central diffraction, we note that in these processes there can be a final state in which one or two deuterons remain intact [see, for example, Fig. 2(c)], which leads to different correlation functions. For example, for Fig. 2(c) the correlation function has the form

$$\begin{aligned}
&C_{\text{Fig. 2(c)}}(L_c|\boldsymbol{p}_{1,T}+\boldsymbol{p}_{2,T}|)\\
&\quad\propto \frac{1}{N_c^2-1}\frac{\int d^2Q_T G_D(Q_T)G_D^2(\boldsymbol{Q}_T-\boldsymbol{p}_{1,T}-\boldsymbol{p}_{2,T})}{\int d^2Q_T G_D(Q_T)G_D(Q_T)}
\end{aligned} \tag{10}$$

which differs from Eq. (6).

A comment regarding the status of the AGK cutting rules in QCD. For deuteron-deuteron scattering, the cutting rules shown in Figs. 3(a)–3(c), have been proved on general grounds [38], using unitarity and the wave nature of the colliding particles. In the framework of perturbative QCD these cutting rules were proven in Refs. [33,39]. For the inclusive cross sections, the AGK cutting rules were discussed and proven in Refs. [40–46]. However, in Ref. [47] it is shown that the AGK cutting rules are violated for double inclusive production. This violation is intimately related to the enhanced diagrams [46,47], and reflects the fact that different cuts of the triple BFKL Pomeron vertex lead to different contributions. Recall, that we do not consider such diagrams.

Therefore, the contribution of the central diffraction process is suppressed by a factor of 4 due to the longitudinal momenta integration. However, we need to compare the values of the vertices for gluon inclusive production [see Fig. 3(d)] and the vertex for two gluon production from the BFKL Pomeron. From Fig. 4 we can see that this vertex is two times larger than the vertex for gluon inclusive production. Indeed, the contribution of Fig. 4(a) is the same

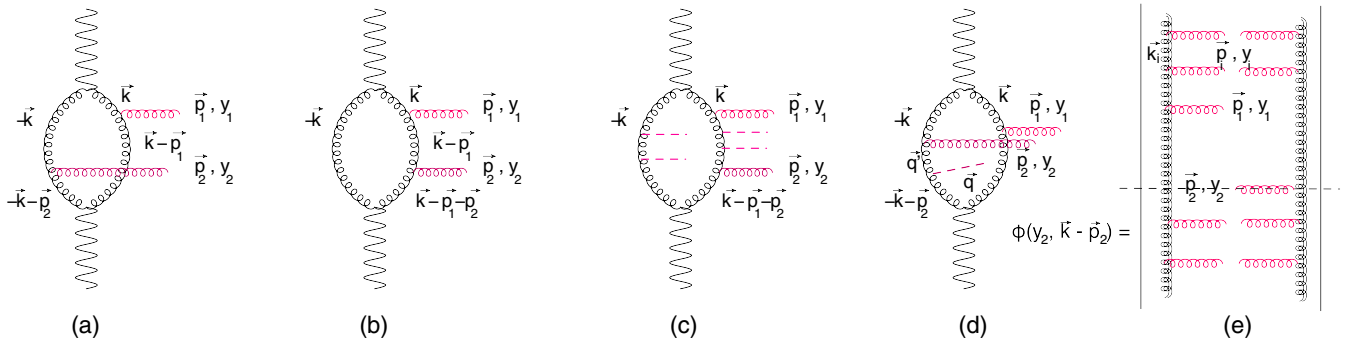

FIG. 4. Vertex for emission of two gluons by the BFKL Pomeron. Fig. 4(c) shows the emission of soft gluons whose suppression leads to the Sudakov form factor. Fig. 4 shows the emission of the gluon in the DLA approximation of perturbative QCD, which leads to the Sudakov form factor in the vertex of two gluons emission.

as for inclusive production, but we have to add Fig. 4b. In Appendix B we show that these two diagrams, Figs. 4(a) and 4(b), are the same. Adding these diagrams, we note that for deuteron-deuteron scattering we expect the symmetry $\varphi \to \pi - \varphi$ in the measurements with no selection on multiplicity. This observation supports the claim of Refs. [15,16].

In this paper as well as in Refs. [15–17] we discuss the case $\bar{\alpha}_S|y_1 - y_2| \le 1$. Let us consider this restriction more carefully. We start with writing the expression for the two diagrams of Fig. 3(d). The inclusive cross section for production of the gluon with rapidity y_1 and transverse momentum $p_{1,T}$ due to the exchange of one BFKL Pomeron has the following form:

$$\frac{d\sigma}{dy_1 d^2p_{T1}} \propto \frac{\bar{\alpha}_S}{p_{1,T}^2}\int d^2k_T \phi^{\rm BFKL}(Y-y_1,k_T) \times \frac{\Gamma_\mu(k_T,p_{1,T})\Gamma_\mu(k_T,p_{1,T})}{k_T^2(\boldsymbol{k}_T-\boldsymbol{p}_{1,T})^2}\phi^{\rm BFKL}(y_1,k_T). \tag{11}$$

The interference diagram in which the parton shower with a gluon with y_1 and $p_{1,T}$ in the amplitude is squared with the parton shower in which a gluon with y_2 and $p_{2,T}$ is produced takes the form

$$\frac{d\sigma}{dy_1 d^2p_{T1}} \propto \frac{\bar{\alpha}_S}{p_{1,T}^2}\int d^2k_T \phi^{\rm BFKL}(Y-y_1,k_T) \times \frac{\Gamma_\mu(k_T,p_{1,T})\Gamma_\nu(k_T,p_{2,T})}{k_T^2(\boldsymbol{k}_T-\boldsymbol{p}_{2,T})^2}\phi^{\rm BFKL}(y_2,k_T). \tag{12}$$

In Eqs. (11) and (12) we neglected $p_{12,T} \propto 1/R_D$ as we have explained above.

In Eqs. (11) and (12) ϕ is the solution of the BFKL equation

$$\frac{\partial\phi^{\rm BFKL}(y,\boldsymbol{k}_T)}{\partial y} = \bar{\alpha}_S\int\frac{d^2k'_T}{\pi}\frac{1}{(\boldsymbol{k}_T-\boldsymbol{k}'_T)^2}\phi^{\rm BFKL}(y,\boldsymbol{k}'_T) - 2\omega_G(\boldsymbol{k}_T)G(y,\boldsymbol{k}_T), \tag{13}$$

where

$$\omega_G(\boldsymbol{k}_T) = \frac{1}{2}\bar{\alpha}_S k_T^2\int\frac{d^2k'_T}{2\pi}\frac{1}{k'^2_T(\boldsymbol{k}_T-\boldsymbol{k}'_T)^2} = \bar{\alpha}_S k_T^2\int\frac{d^2k'_T}{2\pi}\frac{1}{(k'^2_T+(\boldsymbol{k}_T-\boldsymbol{k}'_T)^2)(\boldsymbol{k}_T-\boldsymbol{k}'_T)^2}. \tag{14}$$

Comparing Eqs. (11) and (12), one can see that to neglect the difference between y_2 and y_1 in $\phi^{\rm BFKL}(y_2,k_T)$ we need to assume that $2.8\bar{\alpha}_S|y_1-y_2| \ll 1$ ($2.8\bar{\alpha}_S$ is the intercept of the BFKL Pomeron). However, the actual restriction turns out to be even more severe. Indeed, in all interference diagrams as well as in double gluon production between rapidities y_1 and y_2, we have the exchange in the t channel of two gluons in the octet state. This means that we have the additional emission of gluons with rapidities between y_1 and y_2 [see Fig. 4(c)]. This emission leads to the extra Sudakov form factor [48] in Eq. (12), which takes the form:

$$\frac{d\sigma}{dy_1 d^2p_{T1}} \propto \frac{\bar{\alpha}_S}{p_{1,T}^2}\int d^2k_T e^{-S(\delta y,k_T,p_{1,T})}\phi^{\rm BFKL}(Y-y_1,k_T) \times \frac{\Gamma_\mu(k_T,p_{1,T})\Gamma_\nu(k_T,p_{2,T})}{k_T^2(\boldsymbol{k}_T-\boldsymbol{p}_{2,T})^2}\phi^{\rm BFKL}(y_2,k_T), \tag{15}$$

where $\delta Y = |y_1 - y_2|$. We recall the structure of the one-parton shower that is described by the BFKL Pomeron in Fig. 4(e) [36]; the one-parton shower is given by

$$\prod_{i=1}^{n}\Gamma_\mu(k_{i,T},p_{i,T})\frac{e^{\omega_G(k_{i,T})(y_i-y_{i-1})}}{k^2_{i,T}}, \tag{16}$$

which being squared leads to the parton density $\phi(y,k_{1,T})$. In simple terms, the BFKL cascade is the ladder diagram with specific vertices of gluon production, and with the exchange of the Reggeized gluons with trajectories which are given by Eq. (14). Absorbing the terms in $\phi(y,k_T)$ for Eq. (15), we see that

$$\begin{aligned} S(\delta y,k_T,p_{1,T}) &= (\omega(\boldsymbol{k}_T-\boldsymbol{p}_{1,T})+\omega(\boldsymbol{k}_T))\delta y \\ &= \frac{\bar{\alpha}_S}{2}(\ln((\boldsymbol{k}_T-\boldsymbol{p}_{1,T})^2/\mu^2)+\ln(k_T^2/\mu^2))\delta y, \end{aligned} \tag{17}$$

and it has a typical Sudakov form factor structure. μ is the typical dimensional parameter which in the DGLAP evolution is of the order of the soft scale in the hadron, and in CGC it is a saturation scale $Q_s(y_1\approx y_2)$.

For the diagrams of Figs. 4(a) and 4(b) we need to introduce the same suppressions. These Sudakov suppressions result from the fact that in the approximation for $\bar{\alpha}_S\delta y\ll 1$ we take into account only simple diagrams with two gluons, and without extra gluon emissions, and they stipulate the size we need to take for δy. However, the two-gluon production has an additional suppression of the Sudakov type, which applies even at $y_1=y_2$, where S of Eq. (17) is equal to zero; the emission of gluons that are shown in Fig. 4(d) has been discussed in detail in Ref. [48,49].

This emission leads to the value of S in the double log approximation of perturbative QCD that has the form:

$$S(p_{1,T},k_T)=\frac{\bar{\alpha}_S}{\pi}\int_{k_T}^{M/2}\frac{d^2q_T}{q_T^2}\int_{q_T}^{M/2}\frac{dq_0}{q_0}=\frac{\bar{\alpha}_S}{4}\ln^2\left(\frac{M^2}{4k_T^2}\right), \tag{18}$$

where M denotes the mass of the produced dijet, which is given by $M^2=2p_T^2(1+\cosh(y_1-y_2))$ considering $\boldsymbol{p}_{1,T}=-\boldsymbol{p}_{2,T}=\boldsymbol{p}_T$. The limits in integration over q_0 can easily be understood in the rest frame of the two-gluon jets. In this frame the minimal $q_0=q_T$. The lower limit in q_T integration stems from the fact that at distances less than $1/q_T$, the emission with two t-channel gluons has a destructive interference canceling the emission since the total color charge is zero. For $q_T\geq q_T$ the emission of gluons comes from the t-channel gluon, which carries color, and leads to the color coefficient in Eq. (18).

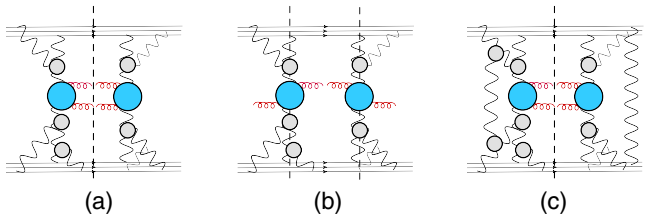

FIG. 5. The double inclusive production for dense-dense parton system scattering: the central diffraction production [see Fig. 5(a)] and the Bose-Einstein correlation of the identical gluons [Fig. 5(b)]. The wavy lines denote the BFKL Pomerons. Figure 5(c) shows the diagrams that do not contribute for the inclusive production of two gluons. The green blobs show the Mueller vertices for two-gluon production, while the circles stand for the triple-Pomeron vertices. The produced gluons are denoted by red helical lines.

Finally, the contribution of the diagram of Fig. 4(b) has the following for $y_1=y_2$:

$$\begin{aligned} &\frac{d\sigma}{dy_1d^2p_{T1}}(\text{Fig.4}(b)) \\ &\propto\frac{\bar{\alpha}_S}{p_{1,T}^2}\int d^2k_Te^{-S(M,k_T)}\phi^{\text{BFKL}}(Y-y_1,k_T) \\ &\times\frac{\Gamma_\mu(\boldsymbol{k}_T,\boldsymbol{p}_{1,T})\Gamma_\nu(\boldsymbol{k}_T-\boldsymbol{p}_{1,T},\boldsymbol{p}_{2,T})}{k_T^2(\boldsymbol{k}_T-\boldsymbol{p}_{1,T})^2}\phi^{\text{BFKL}}(y_1,k_T). \end{aligned} \tag{19}$$

The integration over k_T of the parton densities is concentrated in the vicinity of the saturation scale, since in coordinate space $\phi\propto\nabla^2N(r,y)$ [50], deep in the saturation region it tends to zero. Of course, we consider not only one BFKL Pomeron, but a more complicated structure of the single -parton cascade (see Fig. 5). Therefore, substituting Q_s instead of k_T in the Sudakov form factor, we find that Eq. (19) takes the form:

$$\begin{aligned} \frac{d\sigma}{dy_1d^2p_{T1}}(\text{Fig. 4(b)}) &\propto \frac{\bar{\alpha}_S}{p_{1,T}^2}\exp\left(-\frac{\bar{\alpha}_S}{4}\ln^2\left(\frac{p_T^2(1+\cosh(y_1-y_2))}{2Q_s^2(y_1\approx y_2)}\right)\right) \\ &\times\int d^2k_T\phi^{\text{BFKL}}(Y-y_1,k_T)\frac{\Gamma_\mu(\boldsymbol{k}_T,\boldsymbol{p}_{1,T})\Gamma_\nu(\boldsymbol{k}_T-\boldsymbol{p}_{1,T},\boldsymbol{p}_{2,T})}{k_T^2(\boldsymbol{k}_T-\boldsymbol{p}_{1,T})^2}\phi^{\text{BFKL}}(y_1,k_T). \end{aligned} \tag{20}$$

However, for discussing the current experimental data, especially for hadron-hadron interactions, for the parton densities, we can use the experimental data for DIS structure function, which is well described [51] by the Dokshitzer–Gribov–Lipatov–Altarelli–Parisi (DGLAP) evolution equations [52]. In this case, we need to put the value of $Q_0=Q_s(y_1=Y_0\approx 3)$ from the color glass condensate motivated fit of HERA data [53,54]. This value turns out to be in the range $Q_0=0.2$–0.5 GeV [53,54].

Finally, we obtain the resulting correlation function, which is the sum of Eqs. (6) and (10):

$$C(\varphi) = C(\text{Eq.}(6); L_c 2p_T \sin(\varphi)) + e^{-\frac{\alpha_S}{2}\ln^2\left(\frac{p_T^2(1+\cosh(y_1-y_2))}{2Q_s^2}\right)} C((\text{Eq.}(10); L_c 2p_T \cos(\varphi)), \tag{21}$$

where we assume that $|\boldsymbol{p}_{1,T}| = |\boldsymbol{p}_{2,T}| = p_T$.

The general expectation from Eq. (21) indicates that v_n with odd n will peak at $p_T \approx 4Q_0$, where the second term will be approximately three times smaller that the first one. The experimental data for v_n in proton-proton collisions [55] show that v_n reaches a maximum at $p_T \approx 3$ GeV, and this value is independent of the energy. Such a behavior qualitatively supports Eq. (21) with $Q_0 \approx 0.6$ GeV.

Concluding this section, we would like to summarize our results: (i) We showed that at small transverse momenta the processes of exclusive (diffractive) in the central rapidity region (CED) of two gluons are equal to the interference contributions of two-parton showers, confirming the results of Refs. [15,16]; this fact leads to $v_n = 0$ for odd n in the total inclusive measurements without any selection on multiplicity of produced hadrons. (ii) We found the mechanism of suppression of CED of two-gluon jets for large transverse momenta due to the Sudakov form factor, which leads to the correlation function of Eq. (6), and to $v_n \neq 0$ for odd n in the experiments without selection on multiplicities. (iii) Only the correlation function of Eq. (5) can be measured in the processes of multiparticle generation with the multiplicities $N \geq \bar{n}$, where $\bar{n}$ is the average multiplicity in the collisions. The process of the central diffraction which generates the correlation function of Eq. (6) corresponds to the event with low multiplicity $N < \bar{n}$. The last item is the best motivation for study of the identical particle correlations v_n with even n, and with different multiplicities, which we will consider below.

B. Bose-Einstein correlation function for heavy ions scattering with the correlation length $L_c \propto R_A$

1. Inclusive measurements

Concluding the previous subsection, we claim that for deuteron-deuteron scattering, we see how the processes of the central diffraction in the measurements that sum processes with all possible multiplicities of produced particles can lead to the symmetry $\varphi \to \pi - \varphi$ for $p_T \leq Q_s$. In this section we would like to examine if such symmetry could be possible for ion-ion interactions, which can be described by the Glauber [56] formula [see Fig. 6(a)]:

$$A_{\rm AA}(s,b) = i(1 - \exp(-\Omega(s,b))) \quad \text{with}$$
$$\Omega(s,b) = g_A^2 P^{\rm BFKL}(s,b) T_{\rm AA}(b), \tag{22}$$

where $T_{\rm AA}(b)$ is the optical width and given by

$$T_{\rm AA}(b) = \int d^2b' S_A(\boldsymbol{b} - \boldsymbol{b}') S_A(\boldsymbol{b}') \quad \text{with}$$
$$S_A(b) = \int_{-\infty}^{+\infty} dz \rho(z, \boldsymbol{b}) \int d^2b S_A(b) = A, \tag{23}$$

where $\rho(z, \boldsymbol{b})$ denotes the nucleon density in the nucleus and z the longitudinal coordinate of the nucleon. In Eq. (22) g_N denotes the impact factor that describes the interaction of the BFKL Pomeron (whose Green function is $P^{\rm BFKL}$), with the nucleon.

We wish to stress that Eq. (22) in the framework of perturbative QCD (pQCD) has a region of applicability. Indeed, the contribution of one BFKL Pomeron in pQCD, in Eq. (22), is proportional to $g_N^2 P^{\rm BFKL} T_{\rm AA}(b) \propto \bar{\alpha}_S^2 A^{4/3} \exp(\Delta_{\rm BFKL} Y)$ where $\Delta_{\rm B\,FKL} \propto \bar{\alpha}_S$, where $\Delta_{\rm BFKL}$ denotes the BFKL Pomeron intercept. The first "fan" diagrams lead to corrections to the Glauber formula, which are shown in Fig. 6(b) and are of the order

$$g_N^2 P^{\rm BFKL}(Y) T_{\rm AA}(b) \int_0^Y dy' G_{3IP} g_N P^{\rm BFKL}(y') S_A(b) \propto \bar{\alpha}_S^4 A (P^{\rm BFKL}(Y,b))^2. \tag{24}$$

Comparing Eq. (24) with the exchange of two BFKL Pomerons, we see that the contribution of the fan diagrams will be smaller than 1 for $\Delta_{\rm BFKL} Y \ll \frac{1}{2}\ln(1/(\bar{\alpha}_S^4 A))$, while the contribution of the BFKL Pomeron in Glauber formula will be larger than 1. In other words, for $Y \leq (1/(2\Delta_{\rm BFKL}))\ln(1/(\bar{\alpha}_S^4 A))$ we can describe the ion-ion collisions using the Glauber formula of Eq. (22).

In this formula the contributions of n-BFKL Pomeron exchanges to the total cross section is equal to

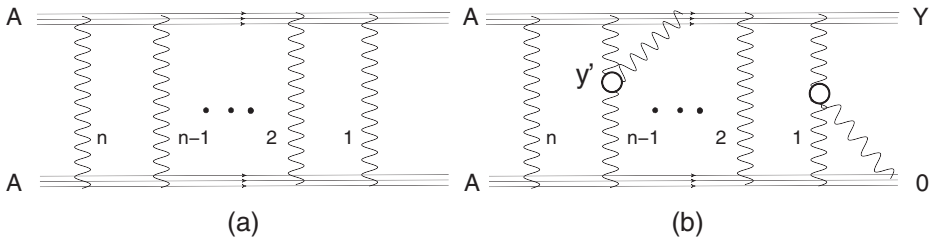

FIG. 6. Nucleus-nucleus scattering in the Glauber [56] approach [Fig. 6(a)], and the first corrections to this approach due to triple–BFKL Pomeron interactions [Fig. 6(b)]. The wavy lines denote the BFKL Pomerons. The blobs show the triple-Pomeron vertices.

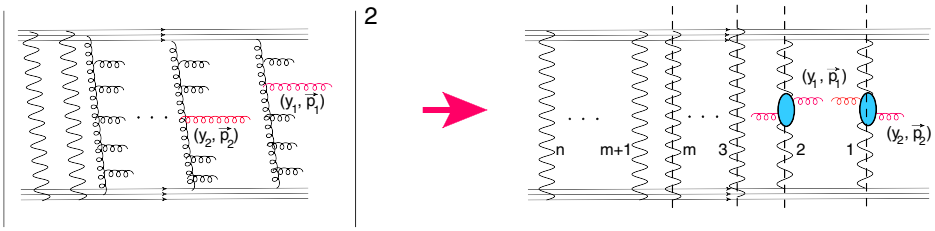

FIG. 7. The contribution of different processes of production of the number of parton showers (more than two), to the Bose-Einstein correlation. The wavy lines denote the BFKL Pomerons. The blobs show the Mueller vertices for two-gluon production. The produced identical gluons are denoted in red helical lines.

$$\sigma^{(n)}_{\rm tot} = \frac{2(-1)^{n-1}}{n!}\Omega^n(s,b). \tag{25}$$

According to the AGK cutting rules, the relative weight of the process with m cut Pomerons ($n-m+1$ of them are not cut) is equal to

$$\frac{\sigma^{(m)}_n}{\sigma^{(n)}_{\rm tot}} = (-1)^{-1-m}\frac{n!}{m!(n-m)!}2^{n-1} \quad \text{for } m \geq 1;$$
$$\frac{\sigma^{(0)}_n}{\sigma^{(n)}_{\rm tot}} = 1 - 2^{n-1}; \tag{26}$$

To find the contribution of all possible processes of different multiplicities[2] related to the production of m-parton showers, we need to calculate the following sum (see Fig. 7):

$$\frac{d^2\sigma}{dy_1 dy_2 d^2p_{T1} d^2p_{T2}} = C_A(L_c|p_{12,T}|)\frac{d\sigma^{\rm BFKL}}{dy_1 d^2p_{T1}}\frac{d\sigma^{\rm BFKL}}{dy_2 d^2p_{T2}} \times \sum_{n=2}^{\infty}\sum_{m=2}^{n} m(m-1)\frac{\sigma^{(m)}_n}{\Omega^2(s,b)} = 4C(L_c|p_{12,T}|)\frac{d\sigma^{\rm BFKL}}{dy_1 d^2p_{T1}}\frac{d\sigma^{\rm BFKL}}{dy_2 d^2p_{T2}}. \tag{27}$$

In Eq. (27) we use Eqs. (26) and (25), and the function C_A is determined by an equation which is similar to Eq. (5). Neglecting all correlations inside the nucleus, its wave function can be written as $\Psi_A(\{r_i\}) = \prod_{i=1}^{A}\Psi_i(r_i)$, where $\Psi(r_i)$ denotes the wave function of ith nucleon. In this approach

$$C_A(L_c|p_{12,T}|) = \frac{1}{N_c^2-1}\frac{\int d^2Q_T G^2_A(Q_T)G^2_A(\boldsymbol{Q}_T - \boldsymbol{p}_{12,T})}{\int d^2Q_T G^4_A(Q_T)}$$
$$\text{with} \quad G_A(Q_T) = \int d^2b e^{i\boldsymbol{b}\cdot\boldsymbol{Q}_T}S_A(b), \tag{28}$$

where $S_A(b)$ denotes the number of the nucleons at fixed impact parameter b.

Equation (28) can be rewritten in the impact parameter representation using Eq. (23), viz.

$$C_A(L_c|p_{12,T}|) = \frac{1}{N_c^2-1}\frac{\int d^2\tilde{b}e^{i\tilde{\boldsymbol{b}}\cdot\boldsymbol{p}_{12,T}}T^2_A(\tilde{b})}{\int d^2\tilde{b}T^2_A(\tilde{b})}$$
$$\text{where } T_A(b) = \int d^2b' S_A(b')S_A(\boldsymbol{b}-\boldsymbol{b}'). \tag{29}$$

The production of gluons by the BFKL Pomerons given by the Mueller diagrams in Fig. 7 generally has a more complicated form than we used in Eq. (27) [see Eq. (38) of Ref. [17]] and cannot be reduced to the production of single inclusive cross sections. However, in the case of deuteron scattering, we can consider $\boldsymbol{p}_{1,T} = \boldsymbol{p}_{2,T}$ since the difference $p_{12,T} \sim 1/R_D \ll 1/R_N$ or $\ll Q_s$, where $1/R_N$ and Q_s are typical momenta in the BFKL Pomeron. Bearing this in mind, we can replace the contribution of the Mueller diagram by the single inclusive production of the gluon with that of the BFKL Pomeron.

The contribution to the central diffraction productions is shown in Fig. 8, and takes the following form:

$$\frac{d^2\sigma}{dy_1 dy_2 d^2p_{T1} d^2p_{T2}} = C_A(L_c|\boldsymbol{p}_{1,T}+\boldsymbol{p}_{2,T}|)\frac{d\sigma^{\rm BFKL}}{dy_1 d^2p_{T1}}\frac{d\sigma^{\rm BFKL}}{dy_2 d^2p_{T2}}\left(\sum_{2}^{n-2}\frac{n!}{2!(n-2)!}\frac{\sigma^{(0)}_n}{\Omega^2(s,b)} + \sum_{n=1}^{\infty}\sum_{m=1}^{n-2}\frac{n!}{2!(n-m-2)!}\frac{\sigma^{(m)}_n}{\Omega^2(s,b)}\right)$$
$$= C_A(L_c|\boldsymbol{p}_{1,T}+\boldsymbol{p}_{2,T}|)\frac{d\sigma^{\rm BFKL}}{dy_1 d^2p_{T1}}\frac{d\sigma^{\rm BFKL}}{dy_2 d^2p_{T2}} \xrightarrow{\Omega\gg 1} 2C_A(L_c|\boldsymbol{p}_{1,T}+\boldsymbol{p}_{2,T}|)\frac{d\sigma^{\rm BFKL}}{dy_1 d^2p_{T1}}\frac{d\sigma^{\rm BFKL}}{dy_2 d^2p_{T2}}. \tag{30}$$

[2]Starting to discuss the multiplicity of the event, we note that we consider the multiplicity in the entire kinematic region in rapidity. However, in the Glauber approach of this section, all our results can be applied for multiplicity in rapidity windows of sizes larger than y_{12}.

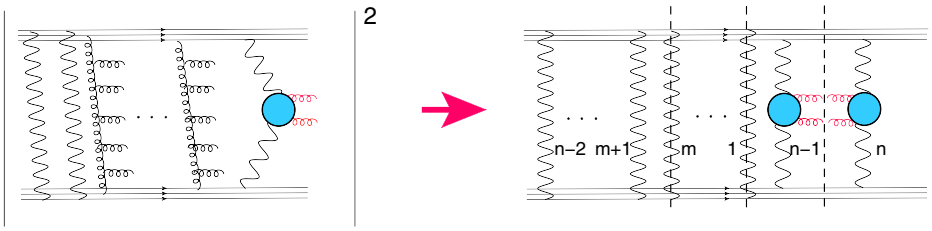

FIG. 8. The contribution of different processes of production of the number of parton showers to the central diffraction production. The wavy lines denote the BFKL Pomerons. The blobs show the Mueller vertices for two-gluon production. The produced gluons are denoted by red helical lines.

In Eq. (30) we use Eqs. (26), (25), and the function $C_A(L_c|\boldsymbol{p}_{1,T}+\boldsymbol{p}_{2,T}|)$ from Eq. (29), as well as $\boldsymbol{p}_{1,T}=-\boldsymbol{p}_{1,2}$ for deuteron-deuteron scattering. Actually, these estimates are correct only in the region of large Ω. The general expression for the correlation function has the following form:

$$C_A(L_c|\boldsymbol{p}_{1,T}+\boldsymbol{p}_{2,T}|) = \frac{1}{N_c^2-1}\frac{\int d^2\tilde{b}e^{i\tilde{\boldsymbol{b}}\cdot(\boldsymbol{p}_{1,T}+\boldsymbol{p}_{2,T})}\int d^2B\int d^2bS_A(\boldsymbol{B}+\frac{1}{2}\tilde{\boldsymbol{b}})S_A(\boldsymbol{B}-\frac{1}{2}\tilde{\boldsymbol{b}})S_A(\boldsymbol{b}+\frac{1}{2}\tilde{\boldsymbol{b}})S_A(\boldsymbol{b}-\frac{1}{2}\tilde{\boldsymbol{b}})(2-\exp(-\Omega(\boldsymbol{b}+\boldsymbol{B})))}{\int d^2\tilde{b}\int d^2B\int d^2bS_A(\boldsymbol{B}+\frac{1}{2}\tilde{\boldsymbol{b}})S_A(\boldsymbol{B}-\frac{1}{2}\tilde{\boldsymbol{b}})S_A(\boldsymbol{b}+\frac{1}{2}\tilde{\boldsymbol{b}})S_A(\boldsymbol{b}-\frac{1}{2}\tilde{\boldsymbol{b}})(2-\exp(-\Omega(\boldsymbol{b}+\boldsymbol{B})))}. \quad (31)$$

We also make use of the fact that the Mueller vertex for production of two gluons by the BFKL Pomeron (see Fig. 8) is equal to the Mueller vertex for inclusive production of a single gluon (see Fig. 7).

Comparing Eqs. (27) and (30), we see that the contribution of the central diffraction production is twice as large (at small p_T) than the contribution of the Bose-Einstein correlations. Therefore, the dominant contribution comes from Eq. (30), leading to the negative values of $v_{n,n}$ for odd n. This prediction contradicts experimental observations. Such a situation could result for two reasons: (1) the measured p_T are larger than typical momentum Q_0, and this contribution is suppressed, as has been discussed in Eq. (21); and (2) the measurements were not made in an inclusive type of the experiment, in which all events were summed without selection on multiplicities of the secondary hadron, but rather only events with large multiplicity were measured.

2. *Measurements with fixed multiplicity $N=m\bar{n}$*

First, we would like to examine what happens to the symmetry $\varphi\to\pi-\varphi$ in an event with given multiplicity. We need to compare the production of m-parton showers which generate the event with multiplicity $N=m\bar{n}$, with the event with the same multiplicity, but in which we produce, in addition, the low multiplicity events by central diffraction production. From the point of view of the AGK cutting rules, the first process is the process with m-cut Pomerons, while the second is the process with the same m-cut Pomerons plus two Pomerons which are not cut. At first sight, the second case could have a larger cross section since it has an additional factor $(\sigma_{\rm in}T_A(b))^2$, which can be large for nucleus-nucleus scattering. We need to estimate this contribution since it is suppressed by factor $\exp(-2\Omega)$ in Eq. (39). In Fig. 9 we plot the b dependence of $\sigma^{(m)}(b)$ of Eq. (39), together with the coefficient from the AGK

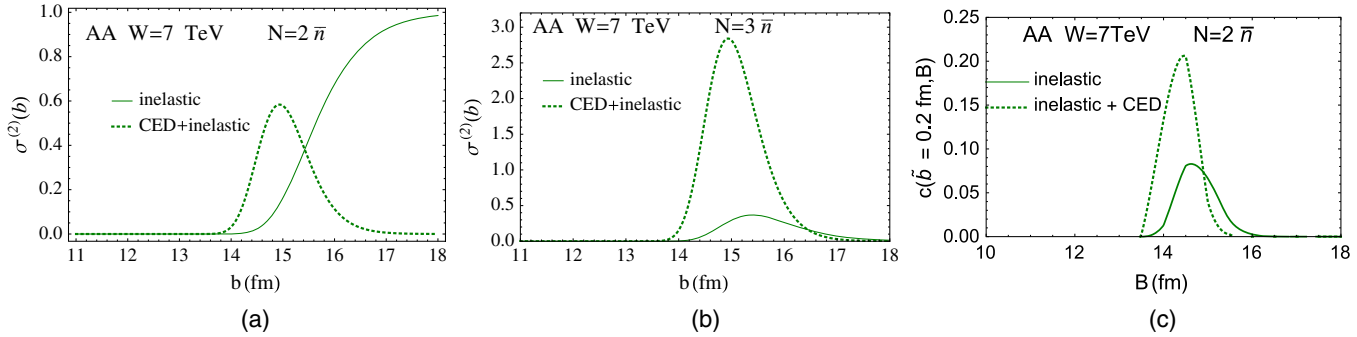

FIG. 9. Comparison of the inelastic events with the multiplicity $N=m\bar{n}$: for the production of two identical gluons from the m-parton showers, and central diffraction production in the event: Fig. 9(a) for m = 2 and Fig. 9(b) for $m=3$. Fig. 9(c) shows the same contribution as Fig. 9(a) after all integrations.

cutting rules. From this figure we see that the process of central diffraction in the inelastic environment is dominant, except for the process with $N = 2\bar{n}$ which needs additional consideration. This fact is a bit surprising since

Inelastic production:

$$N = m\bar{n}\sigma^{(m)}_{\rm in} \propto \frac{m(m-1)}{m!}(2\Omega(b))^{m-2}\exp(-2\Omega(b));$$

Inelastic production + CED:

$$N = m\bar{n}\sigma^{(m)}_{\rm CED} \propto \frac{2}{m!}(2\Omega(b))^{m}\exp(-2\Omega(b)). \quad (32)$$

The survival probability $\exp(-2\Omega(b))$ is very small at all b less than $2R_A$ and determines the value for $2\Omega(b) \leq 1$. Therefore, the extra factor $(2\Omega)^2$ is not an enhancement but a suppression [see Fig. 9(c)]. Nevertheless, it turns out that together with numerical coefficients this kind of suppression does not work.

However, we need to consider the contribution to the correlation function, which includes the additional integrations over impact parameters,

$$\begin{aligned} C(\boldsymbol{p}_{1,T} \pm \boldsymbol{p}_{2,T}) &= \int d^2\tilde{b} e^{i(\boldsymbol{p}_{1,T}\pm\boldsymbol{p}_{2,T})\cdot\tilde{\boldsymbol{b}}}\tilde{c}(\tilde{\boldsymbol{b}}); \\ \tilde{c}(\tilde{\boldsymbol{b}}) &= \int d^2B c(\tilde{\boldsymbol{b}}, \boldsymbol{B}) \\ c(\tilde{\boldsymbol{b}}, \boldsymbol{B}) &= \int d^2b S_A\left(\boldsymbol{B}+\frac{1}{2}\tilde{\boldsymbol{b}}\right)S_A\left(\boldsymbol{B}-\frac{1}{2}\tilde{\boldsymbol{b}}\right)S_A \\ &\times\left(\boldsymbol{b}+\frac{1}{2}\tilde{\boldsymbol{b}}\right)S_A\left(\boldsymbol{b}-\frac{1}{2}\tilde{\boldsymbol{b}}\right)\sigma^{(m)}_{in,\rm CED}(\boldsymbol{B}+\boldsymbol{b}). \end{aligned} \quad (33)$$

Integration over all impact parameters shows that in the event with $N = 2\bar{n}$, the process with dijet production is also larger than the Bose-Einstein correlations [see Fig. 9(c)].

One can see that the multiparticle production accompanied by exclusive production of two-gluon jets prevails, leading to negative $v_{n,n}$ for odd n. For nucleus-nucleus collisions, it is well known that this statement contradicts the experimental data [6,7,11].

3. Measurements with multiplicity $N \geq m\bar{n}$

Hence, for nucleus-nucleus scattering the inclusive experiments, as well as the measurements with fixed multiplicity in the leading $\log(1/x)$ approximation of perturbative QCD, generate negative $v_{n,n}$ for odd n, which contradicts the experimental data. In this subsection we examine the situation when events with multiplicities larger that $m_0\bar{n}$ ($N \geq m_0\bar{n}$) are measured, as has been done in most experiments. Summing Eq. (32) over all $m \geq m_0$, we obtain

$$\begin{aligned} \sigma^{m_0}_{\rm in}(Y;B) &= 1 - \frac{\Gamma(m_0-2, 2\Omega(B;Y))}{\Gamma(m_0-2)} \xrightarrow{\Omega\gg1} 1 \\ &- \frac{(2\Omega(B;Y))^{m_0-3}}{(m_0-3)!}e^{-2\Omega(B;Y)}; \end{aligned} \quad (34)$$

$$\begin{aligned} \sigma^{m_0}_{\rm CED}(Y;B) &= 2\left(1 - \frac{\Gamma(m_0, 2\Omega(B;Y))}{\Gamma(m_0)}\right)\xrightarrow{\Omega\gg1} 2 \\ &\times\left(1 - \frac{(2\Omega(B;Y))^{m_0-1}}{(m_0-1)!}e^{-2\Omega(B;Y)}\right). \end{aligned} \quad (35)$$

One can see that at large Ω, the inelastic event with additional dijet production is larger that the inelastic event that generates the Bose-Einstein correlations. In Fig. 10(a) we plot the function $\tilde{c}(\tilde{b})$ of Eq. (33), which also shows that the inelastic contribution with dijet production prevails. Figure 10(b) shows the correlation functions of Eqs. (6) and (10). Note that the Bose-Einstein correlations are smaller than the correlations due to the diffractive production of dijets.

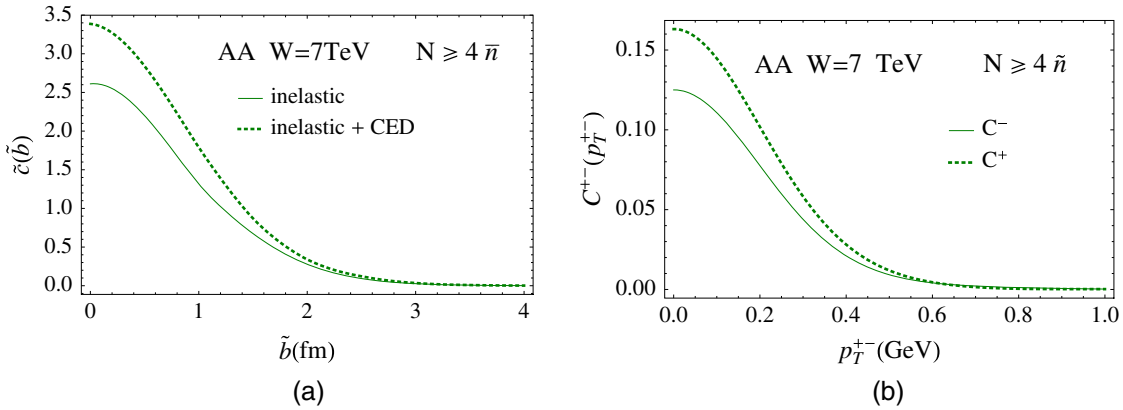

FIG. 10. Comparison of the inelastic events with the multiplicity $N \geq m_0\bar{n}$ in gold-gold collision at $W = 7$ TeV: for the production of two identical gluons for larger than m_0-parton showers, and central diffraction production in the event with multiplicity not smaller than $m_0\bar{n}$. Figure 10(a) shows the contribution of inelastic events and inelastic even plus central diffraction, for $m_0 = 4$. In Fig. 10(b) we plot the correlation functions $C^{\pm}(|\boldsymbol{p}_{1,T} \pm \boldsymbol{p}_{2,T}|)$ [see Eqs. (6) and (10)]. $p^{\pm}_T \equiv |\boldsymbol{p}_{1,T} \pm \boldsymbol{p}_{2,T}|$.

Hence, the experimental results are in direct contradiction with the theoretical predictions based on the leading $\log(1/x)$ approximation of perturbative QCD. The only explanation that we can suggest is that the Sudakov form factor suppresses the dijet production.

We believe that the p measured p_T turns out to be much larger than Q_0, and double log suppression results in a small contribution of the process of central diffraction. Indeed, for the exchange of the BFKL Pomeron our value for $Q_0 \approx Q_s(y_1)$ appears to be overestimated. Our conclusion is that typical $k_T \approx Q_s$ is based on the diagrams of Figs. 5(a) and 5(b), in which the same diagrams contribute to central diffraction and the inclusive cross section. However, for the exclusive central production there no AGK cutting rules, and the diagrams of Fig. 5(c) should be taken into account. If we remove the integral in Eq. (19) for the Sudakov form factor, the remaining expression takes the form of Eq. (20). For the BFKL Pomeron, it is just the contribution to the total cross section. The typical transverse momenta in the BFKL Pomeron both increase and decrease as function of rapidity (see Ref. [57]), and at large y_2 or $Y - y_1$ the typical k_T is as small as the nonpertubative soft momentum, which could be of the order of $\Lambda_{\rm QCD}$. If we replace the emission of gluons by Eq. (20), the diagrams of Fig. 5(c) reduce to the contribution to the total cross section, supporting the idea that Q_0 is of the order of typical soft momentum. Therefore, we expect that $Q_0 \approx \mu_{\rm soft} \approx \Lambda_{\rm QCD}$. Bearing this in mind, we concentrate our efforts below on calculating the Bose-Einstein correlations and their dependence on multiplicity of events.

III. DEPENDENCE OF BOSE-EINSTEIN CORRELATIONS ON THE MULTIPLICITY OF THE EVENT

In this section, we consider the dependence of Bose-Einstein correlations on the multiplicity of the event, using the Glauber formula for the total cross section. In accordance with the AGK cutting rules, the multiplicity of the event (N) is intimately related to the number of parton showers (m) that are produced, where $N = m\bar{n}$.

In the framework of this approach, the Bose-Einstein correlations in the event with multiplicity $N = m\bar{n}$ is determined by the following expression [see also Eq. (33)]:

$$\frac{d^2\sigma}{dy_1 dy_2 d^2p_{T1} d^2p_{T2}} \propto C_A(L_c|\boldsymbol{p}_{12,T}|)\frac{d\sigma^{\rm BFKL}}{dy_1 d^2p_{T1}}\frac{d\sigma^{\rm BFKL}}{dy_2 d^2p_{T2}}; \tag{36}$$

$$C_A(L_c|\boldsymbol{p}_{12,T}|) = \frac{1}{N_c^2-1}\frac{I(L_c|\boldsymbol{p}_{12,T}|)}{I(0)},$$
$$I(L_c|\boldsymbol{p}_{12,T}|) = \int d^2\tilde{b} e^{i\tilde{\boldsymbol{b}}\cdot\boldsymbol{p}_{12,T}}\mathcal{I}(\tilde{b}) \tag{37}$$

$$\mathcal{I}(\tilde{b}) = \int d^2B c(\tilde{\boldsymbol{b}}, \boldsymbol{B}) \tag{38}$$

$$\sigma^{(m)}(\boldsymbol{B}+\boldsymbol{b}) = \sum_{n=m,m\geq 2}^{\infty} m(m-1)\frac{\sigma_n^{(m)}}{\Omega^2(s,\boldsymbol{B})} = \frac{(2\Omega(s,\boldsymbol{B}))^{m-2}}{(m-2)!}e^{-2\Omega(s,\boldsymbol{B})}. \tag{39}$$

If we assume $S_A(b)$ to have a Gaussian form, i.e., $S_A(b) = (A/(\pi R_A^2))\exp(-b^2/R_A^2)$, then Eq. (38) takes the form

$$\mathcal{I}(\tilde{b}) = \left(\frac{A}{\pi R_A^2}\right)^4 e^{-\frac{\tilde{b}^2}{R_A^2}}\left(\int d^2Bd^2b e^{-2\frac{(B^2+b^2)}{R_A^2}}\frac{\sigma_n^{(m)}(\boldsymbol{B}+\boldsymbol{b})}{\Omega^2(s,\boldsymbol{B}+\boldsymbol{b})}\right) \tag{40}$$

and the correlation function does not depend on m, or in other words, it does not depend on the multiplicity of the event. However, this result is the specific property of the Gaussian approximation, which cannot be correct even for hadron-hadron collisions, since it does not lead to the correct exponential behavior of the scattering amplitude at large impact parameters b. Considering the Glauber model for the description of the proton-proton scattering at high energies, we replace S_A and T_A in Eqs. (28) and (29) with

$$S_N(b) = \frac{m^2}{2\pi}K_0(mb);$$
$$T_N = \int d^2b' S_N(b')S_N(\boldsymbol{b}-\boldsymbol{b}');$$
$$\Omega = \sigma_0 e^{\Delta Y}T_N(b), \tag{41}$$

where $\sigma_0 = 4\ 1/\mathrm{GeV}^2$, $m = 1$ GeV, and $\Delta = 0.1$ were chosen to describe the value and energy behavior of the total cross section for the proton-proton interaction at high energy. In Fig. 11(a) the behavior of $\mathcal{I}(b)$ is shown for events with different multiplicities. We see that the correlation length L_c decreases as a function of the multiplicity. In other words, the typical momentum in the correlation function $C(L_c p_{12,T})$ increases with N, as can be seen from Fig. 11(b), where the value of the correlation function $C(L_c p_{12,T})$ is plotted.

The correlation length of the correlation function in nucleus-nucleus collisions shows only mild dependence on the multiplicity of events [see Fig. 12(b)], while the value of $\mathcal{I}$ crucially depends on N [see Fig. 12(a)]. Figure 12(c) shows that the correlation function $C_A(L_c p_{12,T})$ does not depend on the multiplicity of the event.

For completeness of presentation we calculated both $\mathcal{I}(b)$ and $C_{pA}(p_{12,T})$ for proton-gold scattering.

The results of these calculations are plotted in Fig. 13. The first observation is that the correlation length does not depend on the size of the nucleus and is determined by the typical impact parameter in proton-proton scattering. The dependence on multiplicity of the event is rather mild.

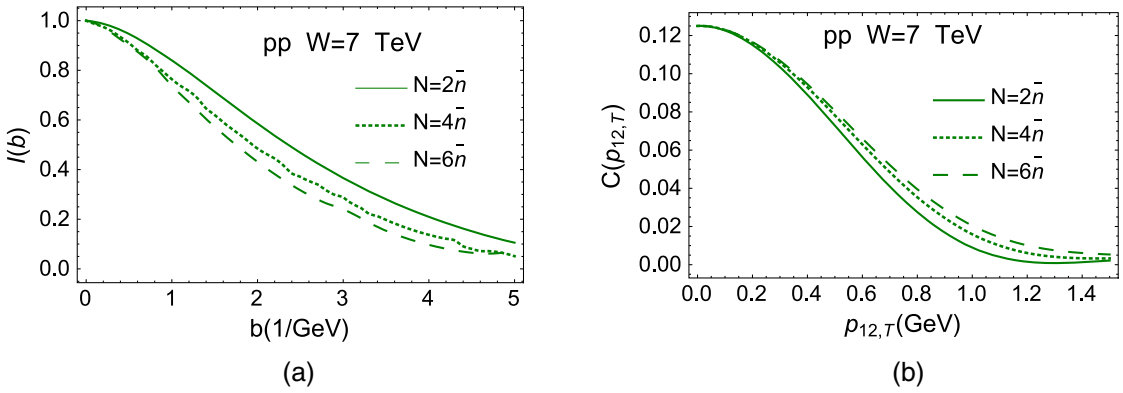

FIG. 11. Figure 11(a) shows $\mathcal{I}(b)$ for proton-proton scattering, with the parameters that are given in Eq. (41), as a function of b for events with different multiplicities normalized to 1 at $b = 0$. In Fig. 11(b) the correlation function $C(p_{12,T})$ is plotted versus $p_{12,T}$. The average multiplicity in the single inclusive production is denoted by $\bar{n}$.

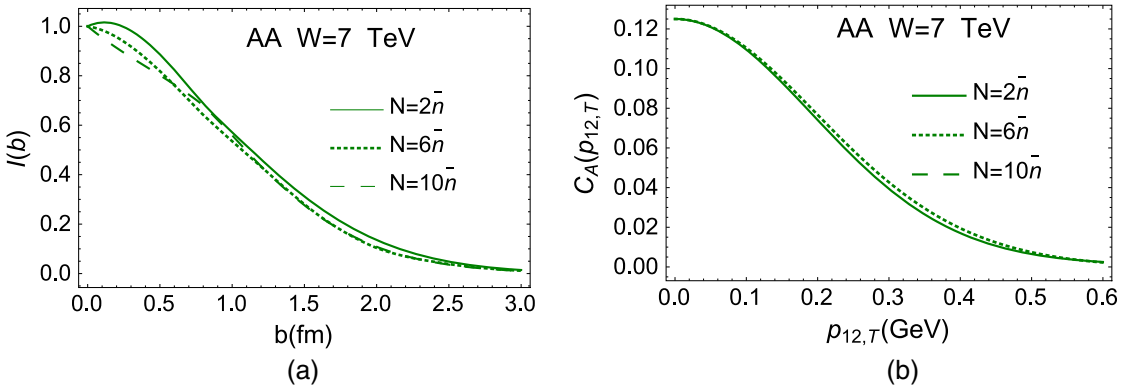

FIG. 12. $\mathcal{I}(b)$ for nucleus-nucleus (gold-gold) scattering with $S_A(b)$ given in Eq. (28) as a function of b for events with different multiplicities. In Fig. 12(a) $\mathcal{I}(b)$ are normalized to their values at $b = 0$. The average multiplicity in the single inclusive production is denoted by $\bar{n}$. The correlation function $C(p_{212,T})$ is plotted in Fig. 12(b).

Concluding this section, we would like to emphasis that the dependence on multiplicity due to the production of several parton showers turns out to be mild, except for the case of hadron-hadron collisions. For this collision the larger the multiplicity of the event, the shorter is the correlation length L_c, or in other words, the typical momentum increases in events with large multiplicities. On the other hand, such an increase is not very pronounced,

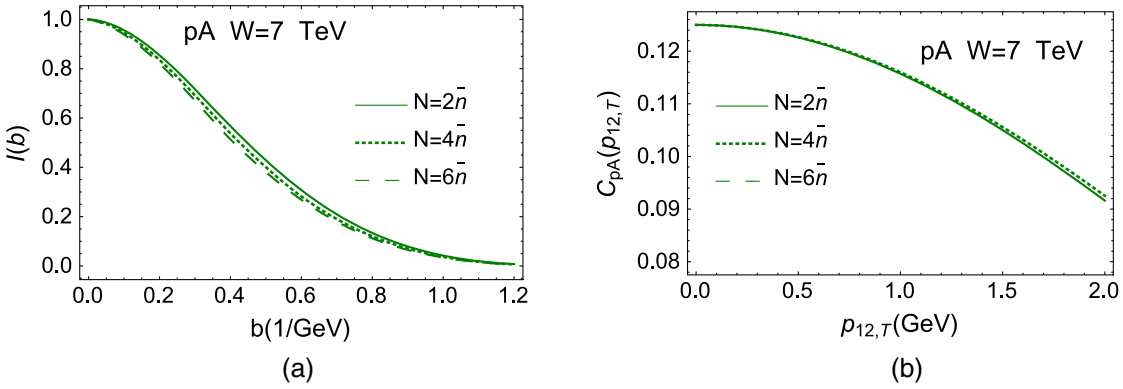

FIG. 13. Fig. 13(a) shows $\mathcal{I}(b)$ for proton-gold scattering with the parameters that are given in Eq. (28), and with the typical $b = 1$ 1/GeV in proton-proton scattering as a function of b for events with different multiplicities, normalized to 1 at $b = 0$. In Fig. 13(b) the correlation function $C_{pA}(p_{12,T})$ is plotted versus $p_{12,T}$. The average multiplicity in the single inclusive production is denoted by $\bar{n}$.

and even for hadron-hadron collisions we can expect that the main source of the multiplicity dependence is from the structure of one-parton showers. In the next section, we discuss the saturation of the parton density in the one-parton shower for nucleus-nucleus collisions, and we develop a simple model in the spirit of the KLN approach.

IV. A SIMPLE KLN-TYPE MODEL FOR THE STRUCTURE OF ONE PARTON CASCADE IN CGC

A. Momentum dependence of the BFKL Pomeron in a nucleus

As we have seen, the diagrams in which the structure of the one-parton shower is described by the BFKL Pomeron lead to a correlation length of azimuthal angle correlations $L_c \propto 1/R_A$, or in other words, to the typical transverse momentum which is very small (see Fig. 12). Therefore, we need to discuss a more complicated structure of the single-parton shower, which is related, for example, to "fan" diagrams shown in Fig. 5(b). We expect that the interaction of the BFKL Pomeron will lead to the value of $L_c \sim 1/Q_{s,A}$, where $Q_{s,A}$ denotes the nucleus saturation momentum. In particular, we consider the diagrams of Figs. 14(a) and 14(b). The diagram of Fig. 14(a) is the first diagram that leads to a correlation function which depends on the saturation momentum of the nucleon, as shown in Refs. [17,21]. We will show that the interaction of the BFKL Pomerons with the nucleus, examples of which are shown in Fig. 14(b), will lead to $L_c \propto 1/Q_{s,A}$.

The general equation for the propagator of the BFKL Pomeron in a nucleus is shown in Fig. 15. The simplest form this equation has is in the framework of Gribov-Pomeron calculus [58] with $\alpha'_{\mathbb{P}} = 0$ and the Pomeron intercept Δ. Denoting the dressed (resulting) propagator of the Pomeron and the solution of the nonlinear Balitsky-Kovchegov equation of Fig. 15(c) by $T_A(Y, Q_T; Y'Q'_T)$ and

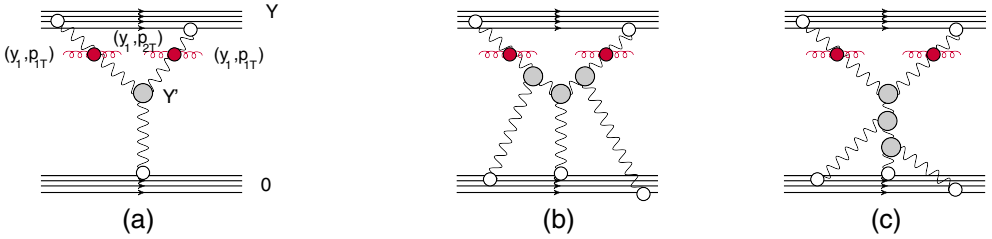

FIG. 14. The double inclusive production for ion-ion collisions which lead to azimuthal correlations with the correlation length $L_c \propto 1/Q_s$: the first diagram is displayed in Fig. 14(a), while Fig. 14(b) shows the interaction of the BFKL Pomerons which results in $L_c \propto 1/Q_{s,A}$, where $Q_{s,A}$ denotes the saturation momentum of the nucleus. The wavy lines denote the BFKL Pomerons. The red blobs show the Mueller vertices for two-gluon production, while the gray circles stand for the triple Pomeron vertices. The white circles show the vertices of the interaction of the BFKL Pomeron with the nucleon in the nucleus. The produced gluons are denoted by red helical lines. For simplicity we draw the diagrams at $y_1 = y_2$.

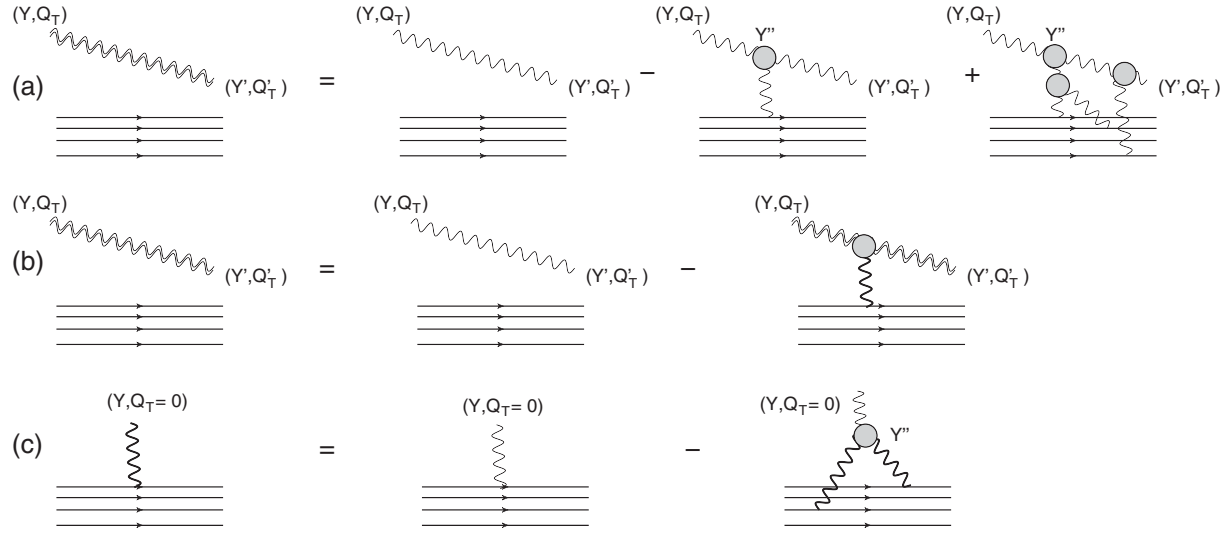

FIG. 15. Equations for BFKL Pomeron propagator in the nucleus. Figure 15(a) shows the first simple diagrams; Fig. 15(b) presents the equation for the propagator; Fig. 15(c) describes the Balitsky-Kovchegov equation. Wavy lines describes the BFKL Pomerons. The double wavy lines denote the resulting propagator. The bold wavy lines stand for the solution of the Balitsky-Kovchegov equation in the nucleus. The blobs denote the triple-Pomeron vertices.

$G_A(Y, Q_T)$, respectively, the equations take the forms

$$T_A(Y, Q_T; Y'Q'_T) = T(Y - Y', Q_T) - \Delta \int_0^Y dY'' d^2Q''_T T(Y - Y'', Q_T) G_A(Y'', \boldsymbol{Q}_T - \boldsymbol{Q}''_T) T_A(Y'', Q''_T; Y'Q'_T); \quad (42)$$

$$\frac{\partial T_A(Y, Q_T; Y'Q'_T)}{\partial Y} = \Delta\left(T_A(Y, Q_T; Y'Q'_T) - \int d^2Q''_T G_A(Y, \boldsymbol{Q}_T - \boldsymbol{Q}''_T) T_A(Y, Q''_T; Y'Q'_T)\right); \quad (43)$$

$$T(Y - Y', Q_T) = g(Q_T) \exp(\Delta(Y - Y')); \qquad T_A(Y = Y', Q_T; Y'Q'_T) = g(Q_T); \quad (44)$$

$$G_A(Y, Q_T) = G(Y - Y', Q_T) - \Delta \int_0^Y dY'' d^2Q''_T G^0(Y - Y'', Q_T) G_A(Y'', \boldsymbol{Q}_T - \boldsymbol{Q}''_T) G_A(Y'', Q''_T; Y'Q'_T); \quad (45)$$

$$\frac{\partial G_A(Y, Q_T)}{\partial Y} = \Delta\left(G_A(Y, Q_T) - \int d^2Q''_T G_A(Y, \boldsymbol{Q}_T - \boldsymbol{Q}''_T) G_A(Y, Q''_T)\right); \quad (46)$$

$$G^0(Y - Y', Q_T) = \exp(\Delta(Y - Y')); \qquad G_A(Y = 0, Q_T) = S_A(Q_T) \quad \text{with} \quad S_A(Q_T) = \int d^2b e^{i\boldsymbol{Q}_T \cdot \boldsymbol{b}} S_A(b). \quad (47)$$

The main idea of solution is the observation that in $G_A(Y, Q_T)$ the typical $Q_T \sim 1/R_A \ll 1/R_N$ or Q_s, where R_N is the nucleon size. Therefore, in Eqs. (42)–(47) we can replace $G_A(Y, Q_T)$ with $\int d^2Q_T G_A(Y, Q_T)\delta^2(Q_T)$. At $Y = 0$, $\int d^2Q_T G_A(Y, Q_T) = S_A(b = 0) \propto 2\rho R_A$, where ρ denotes the density of the nucleons in a nucleus. Plugging this expression into the above equations, they reduce to the following form:

$$\frac{dT_A(Y, Q_T; Y'Q'_T)}{dY} = \Delta(T_A(Y, Q_T; Y'Q'_T) - \tilde{G}_A(Y) T_A(Y, Q_T; Y'Q'_T)); \quad (48)$$

$$\frac{d\tilde{G}_A(Y)}{dY} = \Delta(\tilde{G}_A(Y) - \tilde{G}_A^2(Y)) \quad \text{where } \tilde{G}_A(Y) = \int d^2Q_T G_A(Y, Q_T). \quad (49)$$

Solving Eqs. (49) and (48), we obtain

$$\tilde{G}_A(Y) = \frac{S_A(b=0)e^{\Delta Y}}{1 + S_A(b=0)(e^{\Delta Y} - 1)};$$

$$T_A(Y, Q_T; Y'Q_T) = g(Q_T) e^{\Delta(Y - Y')} \frac{1 + S_A(b=0)(e^{\Delta Y'} - 1)}{1 + S_A(b=0)(e^{\Delta Y} - 1)}. \quad (50)$$

In the general case, the equations have a more complicated structure and include the dependence on the transverse momenta, which are the Fourier images of the dipole sizes. However, in the vicinity of the saturation scale, the scattering amplitude displays a geometric scaling behavior [59] and depends only on one variable, Q_s^2/p_T^2. In the vicinity of the saturation scale the equations take the form [60]:

$$\frac{dT_A(z; z')}{dY} = (1 - \gamma_{cr})(T_A(z, z') - \tilde{G}_A(z) T_A(z, z')); \quad (51)$$

$$\frac{d\tilde{G}_A(z)}{dz} = (1 - \gamma_{cr})(\tilde{G}_A(z) - \tilde{G}_A^2(z)). \quad (52)$$

Solutions of these equations have the following forms:

$$\tilde{G}_A(z) = \frac{\phi_0 e^{(1-\gamma_{cr})z}}{1 + \phi_0(e^{(1-\gamma_{cr})z} - 1)};$$

$$T_A(z, z') = g(Q_T) e^{(1-\gamma_{cr})(z-z')} \frac{1 + \phi_0(e^{(1-\gamma_{cr})z'} - 1)}{1 + \phi_0(e^{(1-\gamma_{cr})z} - 1)}, \quad (53)$$

where ϕ_0 denotes the value of the scattering amplitude at $z = 0$ and

$$z = \ln\left(\frac{Q_{s,A}^2(Y)}{p_T^2}\right) \quad \text{with} \quad Q_{s,A}^2(Y) = S_A(b = 0) Q_s^2(Y), \quad (54)$$

where $Q_S(Y)$ denotes the proton saturation momentum.

The principle feature of all these solutions is that the interaction with the nucleus, which is shown in Fig. 14(b) and in Fig. 15, does not affect the dependence on Q_T, which determines the angular correlations. The only diagrams that could depend on the nuclear saturation momentum are shown in Fig. 14(c). Generally, the BFKL Pomeron from rapidity 0 to rapidity Y' should be replaced by the dressed BFKL Pomeron (see Fig. 16).

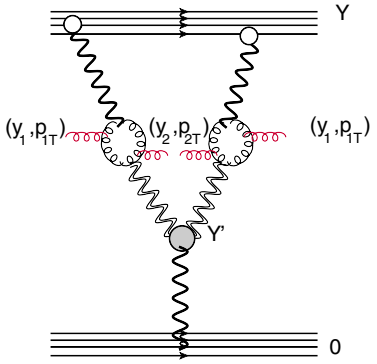

FIG. 16. Double inclusive cross section. The double wavy lines denote the propagator of the dressed BFKL Pomeron. The bold wavy lines stand for the solution of the Balitsky-Kovchegov equation in the nucleus. Helical lines denote gluons.

B. The model

1. The general formulas

The diagram for the interference of two-parton showers is shown in Fig. 16, and can be written in the form

$$\frac{d^2\sigma^{\text{interference diagram}}}{dy_1 dy_2 d^2p_{1,T} d^2p_{2,T}} \propto \frac{\bar{\alpha}_S^2 V^2(p_{1,T}, p_{2,T}, y_1 - y_2)}{p_{1,T}^2 p_{2,T}^2} \times \int_0^{z_1 \approx z_2} dz' G_A(z_Y - z_1) G_A(z_Y - z_2) T_A(z_1 - z') T_A \times (z_2 - z') \Gamma_{3IP}(Q_T; Q_{s,A}(Y')) G_A(z'). \quad (55)$$

Assuming $\bar{\alpha}_S(y_1 - y_2) \ll 1$, $V(p_{1,T}, p_{2,T}, y_1 - y_2)$ takes the simple form

$$V(p_{1,T}, p_{2,T}, y_1 - y_2) = \Gamma_\mu(p_{1,T}, k_T)\Gamma_\mu(p_{2,T}, k_T) \quad (56)$$

with integration over k_T. Since this function does not depend on Q_T, we are not interested in its exact structure. The only function which determines the Q_T is the triple-Pomeron vertex (see Ref. [17]). However, we recall that in inclusive production, the contributions of the BFKL Pomerons with rapidities $Y - y_1(y_2)$ and $y_1(y_2) - Y'$ vanish in the deep saturation region, as they are proportional to $\nabla^2 N(r, \ldots)$ (where r denotes the dipoles size [31,50]), and $N \to 1$ in the saturation region. This means that the contributions of these Pomerons have maxima at $z \to 0$. Therefore, we can use the solutions of Eq. (53) to estimate the value of the cross section.

To specify the Q_T dependence, we need to find which values of z' (or Y') contribute to the integral. Plugging in T_A from Eq. (54), we can take the integral over z', resulting in the following expression:

$$\frac{d^2\sigma^{\text{interference diagram}}}{dy_1 dy_2 d^2p_{1,T} d^2p_{2,T}} \propto e^{2(1-\gamma_{cr})z} \frac{1}{(1 + \phi_0(e^{2(1-\gamma_{cr})z} - 1))^2} \times \left(\frac{(1-\phi_0)}{1-\gamma_{cr}} + \phi_0 z_1 \right). \quad (57)$$

The two terms in Eq. (57) stem from different regions of integration over z'. The first one originates from $z' \to 0$ or $Y' \propto 1/\bar{\alpha}_S$. The second term comes from the region of integration in the entire kinematic region. The typical saturation momentum for such an integration is equal to $\bar{Q}_{s,A}^2 = \sqrt{Q_{s,A}^2(Y_0) Q_{s,A}^2(y_1 \approx y_2)}$.

The dependence on Q_T only comes from the triple-Pomeron vertex. Since $G_A \propto S_A(b)$, the typical Q_T along two upper BFKL Pomerons is equal to zero $Q_T \sim 1/R_A \ll 1/Q_s$, and the dependence on azimuthal angle φ stems from $p_{12,T}^2 = 4p_T^2 \sin(\varphi/2)$. Finally, the general formula for the angular correlations has the form

$$\frac{d^2\sigma}{dy_1 dy_2 d^2p_{1,T} d^2p_{2,T}} \propto \left(\frac{(1-\phi_0)}{1-\gamma_{cr}} \Gamma_{3\mathbb{P}}(Q_T = 0, Q_{s,A}(Y_0)) + \phi_0 z_1 \Gamma_{3\mathbb{P}}(Q_T = 0, \bar{Q}_{s,A}(y_1 \approx y_2)) \right) + \frac{1}{N_c^2 - 1} \left(\frac{(1-\phi_0)}{1-\gamma_{cr}} \Gamma_{3\mathbb{P}}(Q_T = p_{12,T}, Q_{s,A}(Y_0)) + \phi_0 z_1 \Gamma_{3\mathbb{P}}(Q_T = p_{12,T}, \bar{Q}_{s,A}(y_1 \approx y_2)) \right). \quad (58)$$

The triple-Pomeron vertex has been calculated in Ref. [17], and at large Q_T it has the form [see Eq. (45) and Eq. (A12) of Ref. [17]]

$$\Gamma_{3\mathbb{P}}(Q_T, Q_{s,A}) \xrightarrow{Q_T \gg Q_{s,A}} \left(\frac{1}{(\boldsymbol{k}_T - \frac{1}{2}\boldsymbol{Q}_T)^{2\gamma_{cr}} (Q_T^2)^{1-2\gamma_{cr}}} \right)^2 \xrightarrow{Q_T \gg k_T \approx Q_{s,A}} \frac{1}{(Q_T^2)^{2(1-\gamma_{cr})}}, \quad (59)$$

where k_T denotes the momentum inside of the triple-Pomeron vertex, which is of the order of the typical saturation momentum of the lower BFKL Pomeron in Fig. 16. To specify dependence of the triple-Pomeron vertex, we recall that at large impact parameters, the scattering amplitude should decreases exponentially [61]. Bearing this in mind, we suggest that

$$\Gamma_{3\mathbb{P}}(Q_T, Q_{s,A}) = \left(\frac{Q_s^2}{Q_T^2 + Q_s^2} \right)^{2(1-\gamma_{cr})}, \quad (60)$$

which reproduces Eq. (59) at large Q_T and has the exponential decrease at large b.

Plugging Eq. (60) into Eq. (58), we obtain the correlation function in the form

$$C_A(p_{12,T}) = \frac{1}{N_c^2 - 1} \frac{\left(\frac{(1-\phi_0)}{1-\gamma_{cr}}\Gamma_{3\mathbb{P}}(Q_T = p_{12,T}, Q_{s,A}(Y_0)) + \phi_0 z_1 \Gamma_{3\mathbb{P}}(Q_T = p_{12,T}, \bar{Q}_{s,A}(y_1 \approx y_2))\right)}{\left(\frac{(1-\phi_0)}{1-\gamma_{cr}}\Gamma_{3\mathbb{P}}(Q_T = 0, Q_{s,A}(Y_0)) + \phi_0 z_1 \Gamma_{3\mathbb{P}}(Q_T = 0, \bar{Q}_{s,A}(y_1 \approx y_2))\right)}. \tag{61}$$

The multiplicity dependence stems from Eq. (61), where we replace $Q_{S,A}$ with the value of the saturation momentum, which corresponds to the given number of participants, this in the spirit of the KLN approach [27,28]. In Fig. 17 the correlation functions are shown for $W = 5.02$ TeV, and for the choice $Y_0 = \ln(W_0/m)$ with $W = 130$ GeV and $m = 1$ GeV. This function has an essential dependence on $N_{\rm part}$, or on centrality.

v_n can be calculated for $|p_{1,T}| = |p_{2,T}|$ as

$$v_n = \left(\int d\varphi \cos(n\varphi) C_{N_{\rm part}}(2p_T \sin(\varphi/2))\right) \Big/ \left(2\pi + \int d\varphi C_{N_{\rm part}}(2p_T \sin(\varphi/2))\right)^{\frac{1}{2}}. \tag{62}$$

2. The choice of parameters

The formulas of Eqs. (61) and (62) depend only on the value of the saturation momentum, and consequently, it depends on rapidity and $N_{\rm part}$. We follow the KLN approach [23,26,27] in finding these dependences. We assume that

$$Q_s^2(Y; N_{\rm part}) = \frac{\rho_{\rm part}}{2} Q_0^2 e^{\lambda(Y-Y_0)}. \tag{63}$$

The value of Q_0 we fix from the gold-gold scattering at $W = 130$ GeV and for centrality 0–5% $Q_s^2(Y = Y_0) = 2.02$ GeV^2. $Y = \ln(W/W_0)$ and $Y - Y_0 = \ln(W/130)$. $\rho_{\rm part}$ have been calculated in Ref. [23] for the LHC energies, and in Ref. [27] for $W_0 = 130$ GeV. The choice $Y_0 = \ln(W_0/m)$ in Eq. (61) is not theoretically determined; note that the value of typical $\Delta Y'$ in the integral over Y', is about $\Delta Y \sim 1/\bar{\alpha}_S$, and for $\bar{\alpha}_S = 0.2$, this results in a value which is close to the chosen Y_0. Finally, we take $\lambda = 0.25$ as is done in Refs. [23–27].

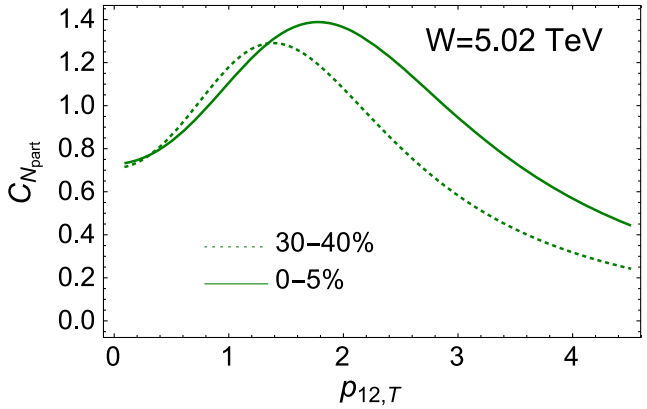

FIG. 17. The correlation function $C_{N_{\rm part}}(p_{12,T})$ at different centralities: 0–5% and 30–40%, versus $p_{12,T}$.

3. Comparison with the experimental data

Using the parameters discussed above, we evaluate the correlation function (see Fig. 17 and the values of v_n which are plotted in Figs. 18, 19, and 20). First, we note that the correlation function depends strongly on the centrality, leading to a correlation length which increases for large centralities.

However, v_n show only mild dependence on centralities (compare Figs. 18 and 19). Such a behavior at first sight is not in accordance with the experimental data. v_2 turns out to be smaller that the experimental values for both centralities. On the other hand, the value for v_2, as well as for other

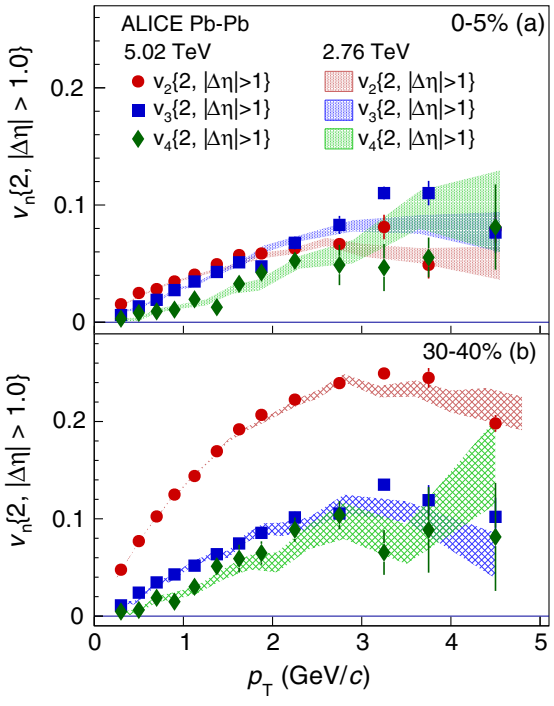

FIG. 18. Experimental data for v_n versus p_T [7] at two different centralities: 0–5% in the upper figure and 30–40% in the lower one.

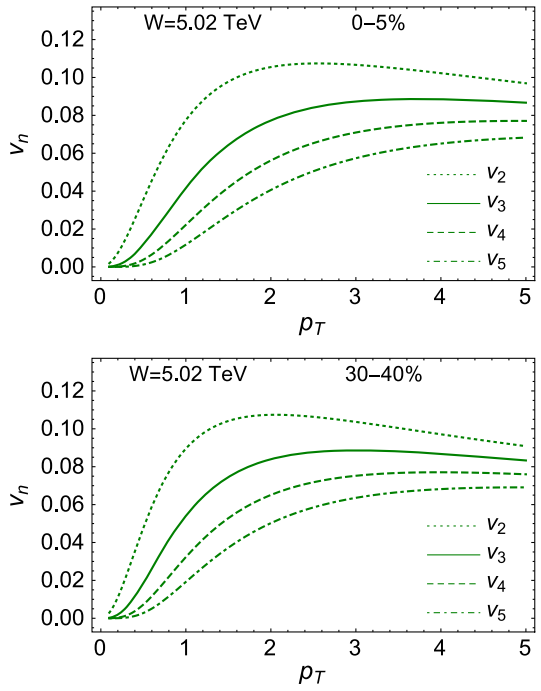

FIG. 19. Our model for v_n versus p_T for different centralities: 0–5% in the upper figure and 30–40% in the lower figure.

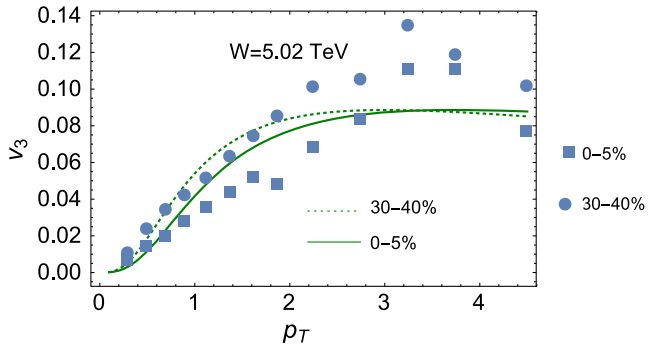

FIG. 20. Comparison of the estimates from our model for v_3 with the experimental data of the ALICE Collaboration [7].

even n, is not very decisive, since in QCD there are many other sources of v_n with even n besides Bose-Einstein correlations. However, we have not found the other sources for v_n with even n. Figure 20 presents our estimate for v_3 together with the experimental data. We see that our predictions for v_3 describe the experimental data fairly well—not extremely well, but the model that we develop here is very simple. These estimates encourage us to develop a more complete description of v_n for even n, with different multiplicities, based on the Bose-Einstein correlations.

V. CONCLUSIONS

We summarize the main results of this paper. The main goal of this paper is to investigate the dependence of Bose-Einstein correlations on the multiplicity of events. We view these correlations as the major source of the azimuthal angle correlations and the only known origin of v_n with odd n in the framework of the color glass condensate. Indeed, the correlation of identical gluons produces the correlation function that depends on $|\boldsymbol{p}_{1,T}-\boldsymbol{p}_{2,T}|$, which gives v_n with odd n. However, in Refs. [15,16] it was noted that the diffractive central production of two different gluons in the colorless state leads to dependence on $|\boldsymbol{p}_{1,T}+\boldsymbol{p}_{2,T}|$. If these two sources have the same strength, the totally inclusive experiments without any selection on multiplicities will give $v_n=0$ for odd n. In this paper, we showed that in the leading $\log(1/x)$ approximation of perturbative QCD the amplitude of two-gluon exclusive production turns out to be equal to the interference diagram, which is the source of the Bose-Einstein correlation, in accordance with Refs. [15,16]. However, the emission of soft gluons for the central exclusive production in the double log approximation of perturbative QCD leads to the Sudakov form factor which suppresses this contribution. Therefore, the Bose-Einstein correlations prevail, leading to $v_n\neq 0$ for odd n. It should be stressed that without this suppression, the measurement of an event with given multiplicity yields $v_{n,n}<0$ for odd n.

We demonstrated that the Bose-Einstein correlation function does not depend on the number of produced parton showers for hadron-nucleus and nucleus-nucleus collisions, but for hadron-hadron collisions such dependence turns out to be considerable.

Finally, we developed a simple KLN-type model to describe the Bose-Einstein correlation in one-parton cascades as a function of centralities. The predicted dependence reflects the main features of the observed data and reproduces the value of v_n with odd n, but much work is still needed to develop a more complete approach. This paper encourages us to search for such an approach.

We view this paper as an argument that the description of v_n is possible due to interactions in the initial state, and that these interactions should not be neglected.

ACKNOWLEDGMENTS

We thank our colleagues at Tel Aviv University and UTFSM for encouraging discussions. Our special thanks go to Carlos Cantreras, Alex Kovner, and Michael Lublinsky for elucidating discussions on the subject of this paper, including drawing our attention to the diagram in Fig. 1(b). This research was supported by the BSF Grant No. 2012124, by Proyecto Basal FB No. 0821 (Chile), Fondecyt (Chile) Grant No. 1140842, and by CONICYT Grant No. PIA ACT1406.

APPENDIX A: INTEGRATION OVER LONGITUDINAL MOMENTA

In this appendix we recall the calculation that results in Eq. (8). For simplicity we restrict ourselves to calculate both the scattering amplitude at high energies [Pomeron, see Figs. 21(a) and 21(b)] and the contribution of the inelastic processes [cut Pomeron, $G(s)$ in Eq. (8), see Fig. 21(c)] in the Born approximation of pQCD. $G(s, t = 0)$ takes the following form [see Fig. 21(c)]:

$$\begin{aligned} G(s,t=0) &= g^4 \mathcal{C} 4 s^2 \int \frac{dk^+ dk_- d^2k_T}{(2\pi)^4 i} \frac{1}{(k^+ k_- - k_T^2 - i\epsilon)^2} 2\pi\delta((P_1 - k)^2) 2\pi\delta((P_2 + k)^2) \\ &= 16 \mathcal{C} \alpha_S^2 s^2 \int dk^+ dk_- d^2k_T \frac{1}{(k^+ k_- - k_T^2 - i\epsilon)^2} \delta(-P_1{}^+ k_- - k_T^2) \delta(P_{2,-} k^+ - k_T^2) \\ &= 32 \mathcal{C} \alpha_S^2 s \int \frac{d^2k_T}{k_T^4}. \end{aligned} \tag{A1}$$

In Eq. (A1) $\mathcal{C}$ is the color coefficient which is the same for all diagrams, factor $4s^2$ [$s = (P_1 + P_2)^2 = 2P_{1,\mu}P_2^\mu$ at high energy] stems from the summation over polarization of the t-channel gluon of the gluon current of quarks $2P_{1,\mu}$ ($2P_{2,\mu}$). $\alpha_S = g^2/4\pi$. Integrating the δ functions, one can see that $k^+ k_- \ll k_T^2$.

The scattering amplitude is equal to

$$\begin{aligned} A(s,t=0) = g^4 \mathcal{C} 4 s^2 \int \frac{dk^+ dk_- d^2k_T}{(2pi)^4 i} \frac{1}{(k^+ k_- - k_T^2 - i\epsilon)^2} \frac{1}{-P_1{}^+ k_- - k_T^2 - i\epsilon} \\ \times \Big(\underbrace{\frac{1}{P_{2,-} k^+ - k_T^2 - i\epsilon}}_{\text{Fig.21}(a)} + \underbrace{\frac{1}{-P_{2,-} k^+ - k_T^2 - i\epsilon}}_{\text{Fig.21}(b)} \Big). \end{aligned} \tag{A2}$$

For $k^+ > 0$ we can take the integral over the pole: $k_-^0 = \frac{-k_T^2 - i\epsilon}{P_1^+}$ closing around this pole, the contour of integration in the lower semiplane in the complex k_- plane, since the integral over a large circle decreases at large k_-. The other pole $k_-^1 = \frac{k_T^2 + i\epsilon}{k^+}$ is located in the upper semiplane. For $k^+ < 0$ all singularities are situated in the lower semiplane leading to vanishing of the integral. Bearing this in mind, we reduce Eq. (A2) to the following expression:

$$\begin{aligned} A(s,t=0) &= \frac{8\alpha_S^2}{\pi} \mathcal{C} s^2 \int_0^\infty dk^+ d^2k_T \frac{1}{k_T^4} \frac{1}{(-P_1^+)} \left(\frac{1}{P_{2,-} k^+ - k_T^2 - i\epsilon} + \frac{1}{-P_{2,-} k^+ - k_T^2 - i\epsilon} \right) \\ &= \frac{8\alpha_S^2}{\pi} \mathcal{C} s^2 \int_{-\infty}^\infty dk^+ d^2k_T \frac{1}{k_T^4} \frac{1}{(-P_1^+)} \frac{1}{P_{2,-} k^+ - k_T^2 - i\epsilon}. \end{aligned} \tag{A3}$$

Taking the integral over k^+ using contour C in Fig. 21(d), and taking into account that the integral over a large circle is equal to $i\pi$, we obtain

$$A(s,t=0) = i 16 \alpha_S^2 \mathcal{C} s \int \frac{d^2k_T}{k_T^4}. \tag{A4}$$

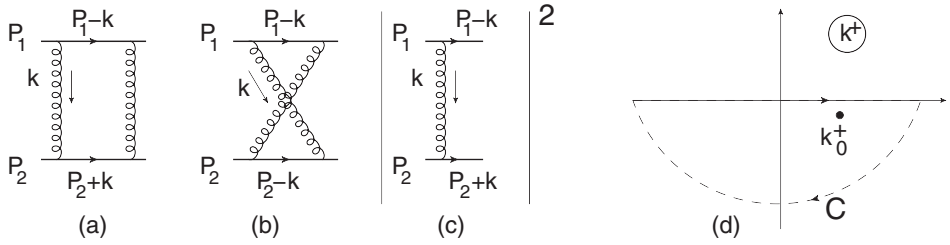

FIG. 21. Born Approximation of pQCD: longitudinal momenta integration. Figs. 21(a) and 21(b) are the diagrams for the scattering amplitude at high energy in the $\bar{\alpha}_S^2$ order of pQCD. Fig. 21(c) is the cross section for two-quark production (cut Pomeron). Fig. 21(d) shows the contour of integration over k^+. Helical lines denote gluons; the solid lines indicate quarks.

The diagram Fig. 21(c) gives the same contribution as the imaginary part of the diagram of Fig. 21(a), multiplied by a factor of 2, since in this diagram we have $2\pi\delta(P_{2,-}k^+ - k_T^2)$. Therefore, we obtain that $2\mathrm{Im}A(s,t=0) = G$ (Fig. 21(c)) which proves Eq. (8) in the Born approximation of pQCD.

For the amplitude of the two-gluon production [see Figs. 22(a) and 22(b)] as well as for the cross section of the one-gluon production, which is shown in Fig. 22(c), we have the following hierarchy of the longitudinal momenta:

$$P_1^+ \gg p_1^+ \sim p_2^+ \gg k^+;$$
$$P_{2,-} \gg p_{1,-} \sim p_{2,-} \gg k_-, \tag{A5}$$

assuming that both gluons are produced with almost equal rapidities ($y_1 \approx y_2$) in the central rapidity region ($y_1 \approx y_2 \ll 1$) in c.m.f.

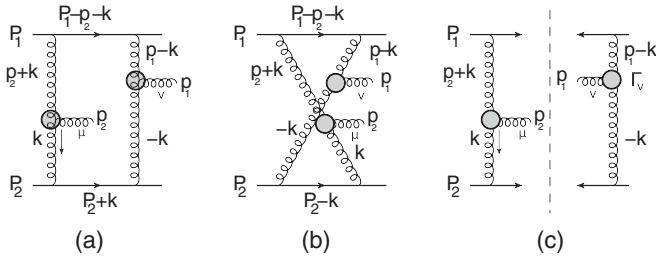

FIG. 22. Born Approximation of pQCD: longitudinal momenta integration. Figs. 22(a) and 22(b) are the diagrams for the amplitude for the production of two gluons with momenta p_1 and p_2, in $\bar{\alpha}_S^3$ order of pQCD. Fig. 22(c) is the cross section for two -quark and two-gluon production (cut Pomeron). Helical lines denote gluons, the solid lines indicate quarks. The blobs denote the Lipatov vertices for gluon production (Γ_ν).

Using Eq. (A5), we can reduce the amplitude to the following expression:

$$\begin{aligned}
&A(\text{Fig.22(a)} + \text{Fig.22(b)}) \\
&= 32\pi\alpha_S^3 \mathcal{C} s^2 \int_0^\infty dk^+ d^2k_T \frac{1}{k_T^4} \frac{\Gamma_\mu(p_{2,T},k_T)}{(\boldsymbol{p}_{2,T}+\boldsymbol{k}_T)^2} \frac{\Gamma_\nu(p_{1,T},k_T)}{(\boldsymbol{p}_{1,T}-\boldsymbol{k}_T)^2} \frac{1}{(-P_1^+)} \left(\frac{1}{P_{2,-}k^+ - k_T^2 - i\epsilon} + \frac{1}{-P_{2,-}k^+ - k_T^2 - i\epsilon} \right) \\
&= 32\alpha_S^3 \mathcal{C} s^2 \int_{-\infty}^\infty dk^+ d^2k_T \frac{1}{k_T^4} \frac{\Gamma_\mu(p_{2,T},k_T)}{(\boldsymbol{p}_{2,T}+\boldsymbol{k}_T)^2} \frac{\Gamma_\nu(p_{1,T},k_T)}{(\boldsymbol{p}_{1,T}-\boldsymbol{k}_T)^2} \frac{1}{(-P_1^+)} \frac{1}{P_{2,-}k^+ - k_T^2 - i\epsilon} \\
&= 32\pi i \alpha_S^3 \mathcal{C} s \int \frac{\Gamma_\mu(p_{2,T},k_T)\Gamma_\nu(p_{1,T},k_T) d^2k_T}{k_T^4 (\boldsymbol{p}_{2,T}+\boldsymbol{k}_T)^2 (\boldsymbol{p}_{1,T}-\boldsymbol{k}_T)^2}.
\end{aligned} \tag{A6}$$

In Eq. (A6) we use the same contour of integration over k^+ [see Fig. 21(d)] as calculating the elastic amplitude [see Eq. (A3)]. The Lipatov vertices Γ_μ for the gluon emission depend only on transverse momenta and do not influence the integration over longitudinal momenta.

The cross section of Fig. 22(c) differs from the amplitude by a factor of 2, which has the same origin as has been discussed above [see Eq. (A1)].

APPENDIX B: VERTICES FOR TWO-GLUON PRODUCTION IN THE CENTRAL RAPIDITY REGION

In this appendix we clarify why diagrams Figs. 4(a) and 4(b) are equal. The vertex in the diagram of Fig. 4(a) has the form

$$V(\text{Fig.4(a)}) = \frac{\Gamma_\mu(\boldsymbol{k}_T,\boldsymbol{p}_{1,T})\Gamma_\nu(-\boldsymbol{k}_T,\boldsymbol{p}_{2,T})}{k_T^2(\boldsymbol{k}_T-\boldsymbol{p}_{2,T})^2}, \tag{B1}$$

while for Fig. 4(b) it can be written as

$$V(\text{Fig.4(b)}) = \frac{\Gamma_\mu(\boldsymbol{k}_T,\boldsymbol{p}_{1,T})\Gamma_\nu(\boldsymbol{k}_T-\boldsymbol{p}_{1,T},\boldsymbol{p}_{2,T})}{k_T^2(\boldsymbol{k}_T-\boldsymbol{p}_{2,T})^2}. \tag{B2}$$

We need to calculate these vertices for $\boldsymbol{p}_{1,T} = -\boldsymbol{p}_{2,T}$, since $|\boldsymbol{p}_{1,T}+\boldsymbol{p}_{2,T}| \propto 1/R_D \ll 1/R_N$.

The vertices Γ_μ have the following expressions:

$$\begin{aligned}
\Gamma_\mu(\boldsymbol{k}_T,\boldsymbol{p}_{1,T}) &= \frac{1}{p_{1,T}^2}(k^2\boldsymbol{p}_{1,T} - p_{1,T}^2\boldsymbol{k}_T); \\
\Gamma_\nu(\boldsymbol{k}_T-\boldsymbol{p}_{1,T},\boldsymbol{p}_{2,T}) &= \frac{1}{p_{2,T}^2}((\boldsymbol{k}-\boldsymbol{p}_{1,T})^2\boldsymbol{p}_{2,T} - p_{2,T}^2(\boldsymbol{k}_T-\boldsymbol{p}_{1,T})).
\end{aligned} \tag{B3}$$

We need to convolute these vertices with $\Gamma_\mu(\boldsymbol{l}_T,\boldsymbol{p}_{1,T})$ and $\Gamma_\nu(\boldsymbol{l}_T-\boldsymbol{p}_{1,T},\boldsymbol{p}_{2,T})$ for the different Pomerons, where the integration is over l_T. In such convolution the terms that are

proportional to $\boldsymbol{p}_{1,T}\cdot\boldsymbol{k}_T$ or to $\boldsymbol{p}_{1,T}\cdot\boldsymbol{l}_T$ vanish due to angular integrations. Only the term which is proportional to $(\boldsymbol{k}_T\cdot\boldsymbol{l}_T)^2$ survives and yields $\frac{1}{2}l_T^2k_T^2$. It is easy to see that this term is the same in both vertices of Eqs. (B1) and (B2). Now we need to compare

$$\Gamma_\mu(\boldsymbol{k}_T,\boldsymbol{p}_T)\cdot\boldsymbol{p}_T=\frac{1}{p_T^2}(k^2\boldsymbol{p}_T-p_T^2\boldsymbol{k}_T)\cdot\boldsymbol{p}_T \tag{B4}$$

with

$$\Gamma_\nu(\boldsymbol{k}_T-\boldsymbol{p}_T,\boldsymbol{p}_T)=\frac{1}{p_T^2}((\boldsymbol{k}-\boldsymbol{p}_T)^2\boldsymbol{p}_T+p_T^2(\boldsymbol{k}_T-\boldsymbol{p}_T))\cdot\boldsymbol{p}_T, \tag{B5}$$

where we denote $\boldsymbol{p}_{1,T}=\boldsymbol{p}_T=-\boldsymbol{p}_{2,T}$.

The direct calculations give the same expression for both terms,

$$\frac{1}{2}p_T^2((\boldsymbol{k}_T-\boldsymbol{p}_T)^2+k_T^2-p_T^2). \tag{B6}$$

Therefore, both diagrams give the same contribution.

[1] V. Khachatryan *et al.* (CMS Collaboration), Phys. Rev. Lett. **116**, 172302 (2016); J. High Energy Phys. 09 (2010) 091.
[2] J. Adams *et al.* (STAR Collaboration), Phys. Rev. Lett. **95**, 152301 (2005).
[3] B. Alver *et al.* (PHOBOS Collaboration), Phys. Rev. Lett. **104**, 062301 (2010).
[4] H. Agakishiev *et al.* (STAR Collaboration), arXiv: 1010.0690.
[5] S. Chatrchyan *et al.* (CMS Collaboration), Phys. Lett. B **718**, 795 (2013); V. Khachatryan *et al.* (CMS Collaboration), J. High Energy Phys. 09 (2010) 091.
[6] S. Chatrchyan *et al.* (CMS Collaboration), J. High Energy Phys. 02 (2014) 088; Phys. Rev. C **89**, 044906 (2014); Eur. Phys. J. C **72**, 2012 (2012).
[7] J. Adam *et al.* (ALICE Collaboration), Phys. Rev. Lett. **117**, 182301 (2016); **116**, 132302 (2016); L. Milano (ALICE Collaboration), Nucl. Phys. **A931**, 1017 (2014); Y. Zhou (ALICE Collaboration), J. Phys. Conf. Ser. **509**, 012029 (2014).
[8] B. B. Abelev *et al.* (ALICE Collaboration), Phys. Rev. C **90**, 054901 (2014); Phys. Lett. B **726**, 164 (2013); **719**, 29 (2013).
[9] G. Aad *et al.* (ATLAS Collaboration), Phys. Rev. Lett. **116**, 172301 (2016).
[10] G. Aad *et al.* (ATLAS Collaboration), Phys. Rev. C **90**, 044906 (2014); B. Wosiek (ATLAS Collaboration), Ann. Phys. (Amsterdam) **352**, 117 (2015); G. Aad *et al.* (ATLAS Collaboration), Phys. Lett. B **725**, 60 (2013).
[11] B. Wosiek (ATLAS Collaboration), Phys. Rev. C **86**, 014907 (2012).
[12] E. M. Levin, M. G. Ryskin, and S. I. Troian, Yad. Fiz. **23**, 423 (1976) [Sov. J. Nucl. Phys. **23**, 222 (1976)]; A. Capella, A. Krzywicki, and E. M. Levin, Phys. Rev. D **44**, 704 (1991).
[13] E. Gotsman, E. Levin, and U. Maor, Phys. Rev. D **95**, 034005 (2017).
[14] A. Kovner and M. Lublinsky, Phys. Rev. D **83**, 034017 (2011).
[15] Y. V. Kovchegov and D. E. Wertepny, Nucl. Phys. **A906**, 50 (2013).
[16] T. Altinoluk, N. Armesto, G. Beuf, A. Kovner, and M. Lublinsky, Phys. Lett. B **752**, 113 (2016); **751**, 448 (2015).
[17] E. Gotsman and E. Levin, Phys. Rev. D **95**, 014034 (2017).
[18] A. Kovner, M. Lublinsky, and V. Skokov, Phys. Rev. D **96**, 016010 (2017).
[19] K. Dusling and R. Venugopalan, Phys. Rev. D **87**, 094034 (2013), and references therein.
[20] A. Kovner and M. Lublinsky, Int. J. Mod. Phys. E **22**, 1330001 (2013), and references therein.
[21] E. Gotsman, E. Levin, and U. Maor, Eur. Phys. J. C **76**, 607 (2016).
[22] A. Dumitru, D. E. Kharzeev, E. M. Levin, and Y. Nara, Phys. Rev. C **85**, 044920 (2012).
[23] D. Kharzeev, E. Levin, and M. Nardi, Nucl. Phys. **A747**, 609 (2005).
[24] D. Kharzeev, E. Levin, and M. Nardi, Nucl. Phys. **A730**, 448 (2004); **A743**, 329(E) (2004).
[25] D. Kharzeev, E. Levin, and M. Nardi, Phys. Rev. C **71**, 054903 (2005).
[26] D. Kharzeev, E. Levin, and L. McLerran, Phys. Lett. B **561**, 93 (2003).
[27] D. Kharzeev and E. Levin, Phys. Lett. B **523**, 79 (2001).
[28] D. Kharzeev and M. Nardi, Phys. Lett. B **507**, 121 (2001).
[29] R. Hanbury Brown and R. Q. Twiss, Nature (London) **178**, 1046 (1956).
[30] G. Goldhaber, W. B. Fowler, S. Goldhaber, and T. F. Hoang, Phys. Rev. Lett. **3**, 181 (1959); G. I. Kopylov and M. I. Podgoretsky, Yad. Fiz. **15**, 392 (1972) [Sov. J. Nucl. Phys. **15**, 219 (1972)]; G. Alexander, Rep. Prog. Phys. **66**, 481 (2003).
[31] Y. V. Kovchegov and E. Levin, *Quantum Choromodynamics at High Energies*, Cambridge Monographs on Particle Physics, Nuclear Physics and Cosmology (Cambridge University Press, Cambridge, England, 2012).
[32] V. A. Abramovsky, V. N. Gribov, and O. V. Kancheli, Yad. Fiz. **18**, 595 (1973) [Sov. J. Nucl. Phys. **18**, 308 (1974)].
[33] L. V. Gribov, E. M. Levin, and M. G. Ryskin, Phys. Rep. **100**, 1 (1983).
[34] E. M. Levin and M. G. Ryskin, Phys. Rep. **189**, 268 (1990).
[35] A. H. Mueller, Phys. Rev. D **2**, 2963 (1970).

[36] E. A. Kuraev, L. N. Lipatov, and V. S. Fadin, Sov. Phys. JETP **45**, 199 (1977); Y. Y. Balitsky and L. N. Lipatov, Sov. J. Nucl. Phys. **28**, 22 (1978).
[37] L. N. Lipatov, Sov. Phys. JETP **63**, 904 (1986) [Zh. Eksp. Teor. Fiz **90**, 1536 (1986)].
[38] E. M. Levin and M. G. Ryskin, Yad. Fiz. **25**, 849 (1977).
[39] J. Bartels and M. G. Ryskin, Z. Phys. C **76**, 241 (1997).
[40] Y. V. Kovchegov, Phys. Rev. D **64**, 114016 (2001); **68**, 039901(E) (2003).
[41] Y. V. Kovchegov and K. Tuchin, Phys. Rev. D **65**, 074026 (2002).
[42] J. Jalilian-Marian and Y. V. Kovchegov, Phys. Rev. D **70**, 114017 (2004); **71**, 079901(E) (2005).
[43] M. A. Braun, Eur. Phys. J. C **48**, 501 (2006).
[44] C. Marquet, Nucl. Phys. **B705**, 319 (2005).
[45] A. Kovner and M. Lublinsky, J. High Energy Phys. 11 (2006) 083.
[46] E. Levin and A. Prygarin, Phys. Rev. C **78**, 065202 (2008).
[47] J. Jalilian-Marian and Y. V. Kovchegov, Phys. Rev. D **70**, 114017 (2004); **71**, 079901(E) (2005).
[48] V. A. Khoze, A. D. Martin, and M. G. Ryskin, Eur. Phys. J. C **48**, 467 (2006); **14**, 525 (2000); Phys. Rev. D **56**, 5867 (1997); **401**, 330 (1997).
[49] Y. L. Dokshitzer, D. Diakonov, and S. I. Troian, Phys. Rep. **58**, 269 (1980).
[50] Y. V. Kovchegov and K. Tuchin, Phys. Rev. D **65**, 074026 (2002).
[51] H. Abramowicz *et al.* (ZEUS Collaboration), Phys. Rev. D **93**, 092002 (2016); H. Abramowicz *et al.* (H1 and ZEUS Collaborations), Eur. Phys. J. C **75**, 580 (2015).
[52] V. N. Gribov and L. N. Lipatov, Sov. J. Nucl. Phys. **15**, 438 (1972); L. N. Lipatov, Yad. Fiz. **20**, 181 (1974); G. Altarelli and G. Parisi, Nucl. Phys. **B126**, 298 (1977); Yu. L. Dokshitser, Sov. Phys. JETP **46**, 641 (1977).
[53] J. L. Albacete, N. Armesto, J. G. Milhano, P. Quiroga-Arias, and C. A. Salgado, Eur. Phys. J. C **71**, 1705 (2011).
[54] E. Iancu, J. D. Madrigal, A. H. Mueller, G. Soyez, and D. N. Triantafyllopoulos, Phys. Lett. B **750**, 643 (2015).
[55] G. Aad *et al.* (ATLAS Collaboration), Phys. Rev. Lett. **116**, 172301 (2016).
[56] R. J. Glauber, in *Lectures in Theoretical Physics*, edited by W. E. Brittin and L. G. Duham (Interscience, New York, 1959), Vol. 1.
[57] J. Bartels, J. Phys. G **19**, 1611 (1993).
[58] V. N. Gribov, Zh. Eksp. Teor. Fiz. **53**, 654 (1967) [Sov. Phys. JETP **26**, 414 (1967)].
[59] J. Bartels and E. Levin, Nucl. Phys. **B387**, 617 (1992); E. Iancu, K. Itakura, and L. McLerran, Nucl. Phys. **A708**, 327 (2002).
[60] A. H. Mueller and D. N. Triantafyllopoulos, Nucl. Phys. **B640**, 331 (2002); D. N. Triantafyllopoulos, Nucl. Phys. **B648**, 293 (2003).
[61] M. Froissart, Phys. Rev. **123**, 1053 (1961); A. Martin, Lect. Notes Phys. **3**, 1 (1969).